

Exotic populations in Galactic Globular Clusters

Francesco R. Ferraro

*Dipartimento di Astronomia, Università di Bologna, Via Ranzani 1,
 40127 Bologna (ITALY)*

Abstract. Recent high-resolution observations of the central region of Galactic globular clusters have shown the presence of a large variety of exotic stellar objects whose formation and evolution may be strongly affected by dynamical interactions. In this paper I review the main properties of two classes of exotic objects: the so-called Blue Stragglers stars and the recently identified optical companions to Millisecond pulsar. Both these class of objects are invaluable tools to investigate the binary evolution in very dense environments and are powerful tracers of the dynamical history of the parent cluster.

1. Introduction

Ultra-dense cores of Galactic Globular Clusters (GCs) are very efficient “furnaces” for generating exotic objects, such as low-mass X-ray binaries, cataclysmic variables, millisecond pulsars (MSPs), blue stragglers (BSS), etc. Most of these objects are thought to result from the evolution of various kinds of binary systems originated and/or hardened by stellar interactions. The nature and even the existence of binary by-products can be strongly affected by the cluster core dynamics, thus serving as a diagnostic of the dynamical evolution of GCs. This topic has received strong impulse in the recent years and many studies have been devoted to investigate the possible link between the dynamical evolution of clusters and the evolution of their stellar population.

In particular two aspects can be investigated: (1) the environment effects on canonical evolutionary sequences (as for example the possible effect of different environments on the blue tail extension of the Horizontal Branch - HB, see Fusi Pecci et al 1992, Buonanno et al 1997); (2) the creation of artificial sequences as BSS and other exotic objects (see Bailyn 1995 and reference therein).

In this paper I will review the main properties of two anomalous sequences in the color-magnitude diagram (CMD):

- the most known *anomalous sequence* in GCs: the so-called BSS sequence, indeed the very first sequence of exotic objects discovered in the CMD of GCs;
- the most recently discovered *anomalous sequence*: the one defined by MSP companions.

2. Blue Straggler Stars

BSS, first discovered by Sandage (1953) in M3, are commonly defined as stars brighter and bluer (hotter) than the main sequence (MS) turnoff (TO), lying along an apparent extension of the MS, and thus mimicking a rejuvenated stellar population. The existence of such a population has been a puzzle for many years, and even now its formation mechanism is not completely understood, yet. At present, the leading explanations involve mass transfer between binary companions, the merger of a binary star system or the collision of stars (whether or not in a binary system). Direct measurements (Shara et al. 1997) and indirect evidence show that BSS are more massive than the normal MS stars, pointing again towards collision or merger of stars. Thus, BSS represent the link between classical stellar evolution and dynamical processes (see Bailyn 1995). The realization that BSS are the ideal diagnostic tool for a quantitative evaluation of the dynamical interaction effects inside star clusters has led to a remarkable burst of searches and systematic studies, using UV and optical broad-band photometry.

2.1. The UV approach to the study of BSS

The observational and interpretative scenario of BSS has significantly changed in the last 20 years. In fact, since their discovery and for almost 40 years, BSS have been detected only in the outer regions of GCs or in relatively loose clusters, thus forming the idea that a low-density environment is the *natural habitat* for BSS. Of course, it was an observational bias: starting from the early '90 high resolution studies allowed to properly image the central region of high density clusters (see the case of NGC6397 by Auriere & Ortolani 1990). Moreover, with the advent of the Hubble Space Telescope (HST) it became possible for the first time to search dense cluster cores for BSS. This was a really turning point in BSS studies since HST, thanks to its unprecedented spatial resolution and imaging/spectroscopic capabilities in the UV, has given a new impulse to the study of BSS (see Paresce et al 1992, Paresce & Ferraro (1993), Guhatakurtha et al 1994, etc).

Based on these observations, the first catalogs of BSS have been published (Fusi Pecci et al 1992; Sarajedini 1992; Ferraro, Bellazzini & Fusi Pecci 1995, hereafter FFB95) until the most recent collection of BSS which counts nearly 3000 candidates (Piotto et al 2004). These works have significantly contributed to form the nowadays, commonly accepted idea that BSS are a normal stellar population in clusters, since they are present in all of the properly observed GCs. However, according to Fusi Pecci et al. (1992) BSS in different environments could have different origin. In particular, BSS in loose GCs might be produced from coalescence of primordial binaries, while in high density GCs (depending on survival-destruction rates for primordial binaries) BSS might arise mostly from stellar interactions, particularly those which involve binaries. Thus, while the suggested mechanisms for BSS formation could be at work in clusters with different environments (FFB95; Ferraro et al. 1999), there are evidence that they could also act simultaneously within the same cluster (as in the case of M3, see Ferraro et al. 1993 - hereafter F93; Ferraro et al. 1997 - hereafter F97). Moreover, as shown by Ferraro et al. (2003 - hereafter F03), both the BSS formation channels (primordial binary coalescence and stellar interactions)

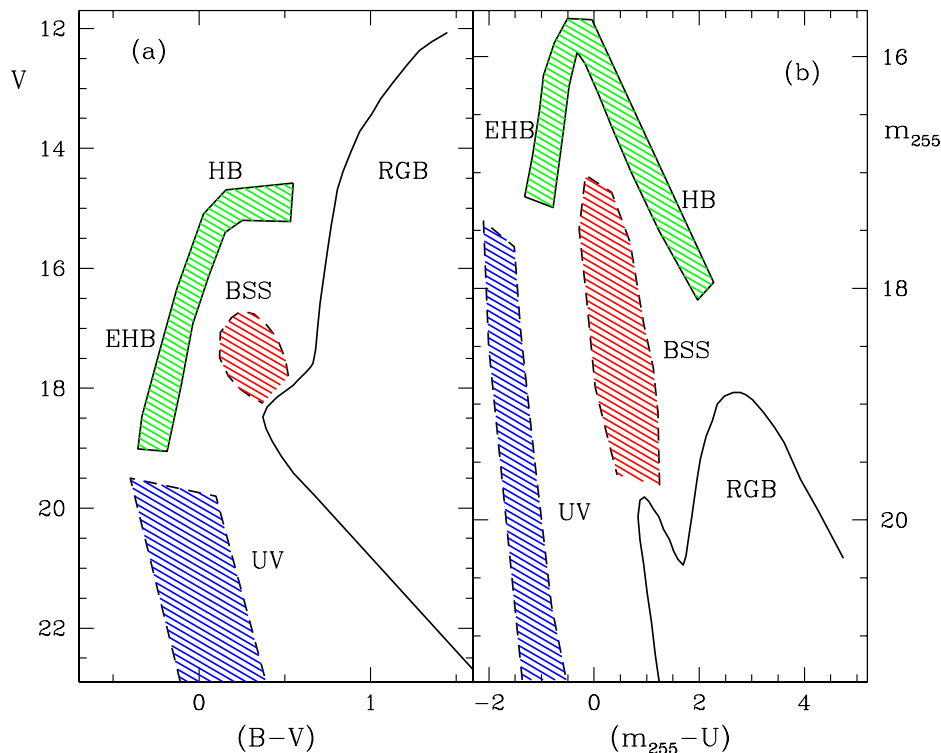


Figure 1. The main sequences of a GC CMD in the $(V, B-V)$ and $(m_{255}, m_{255} - U)$ -planes, respectively.

seem to be equally efficient in producing BSS in different environments, since the two clusters that show the largest known BSS specific frequency, i.e. NGC 288 (Bellazzini et al. 2002) and M 80 (Ferraro et al. 1999), represent two extreme cases of central density concentration among the GCs ($\text{Log} \rho_0 = 2.1$ and 5.8, respectively).

However, a major problem in the systematic study of the BSS still persists, especially in the central region of high density clusters by using the classical CMD even with HST. In fact, the CMD of an old stellar population (as a GC) in the *classical* $(V, B - V)$ plane is dominated by the cool stellar component, hence the observations and the construction of complete sample of hot stars (as extreme blue HB, BSS, various by-products of binary system evolution etc.) is “intrinsically” difficult in this plane. Moreover, in visible CMDs the BSS region could be severely affected by photometric blends which mimic BSS.

In the ultraviolet (UV) plane, where the sub-giants and red giant stars which cause BSS-like blends are faint and the hot stellar populations are relatively

bright, problems are much less severe, allowing to obtain complete BSS samples even in the densest cluster core regions. The advantage of studying BSS in the mid-UV CMD is shown in Figure 1, where the shapes of the main evolutionary sequences in the traditional (V,B-V) plane (*panel (a)*) and in the UV plane (*panel (b)*) are compared. As can be seen, in the UV plane the main branches display very different morphologies with respect to those in the optical CMD (i.e. V , $V - I$). As can be seen, the red giant branch (RGB) is very faint in the UV, while the HB, excluding the hottest section, which bends downward because of the increasing bolometric correction, appears diagonal. Since red giants are faint in UV, the photometric blends, which mimic BSS in visible CMDs, are less problematic. The BSS define a narrow, nearly vertical sequence spanning ~ 3 mag in this plane, thus, a complete BSS sample can be obtained even in the densest cores: indeed, the $(m_{255}, m_{255} - m_{336})$ plane is an ideal tool for selecting BSS.

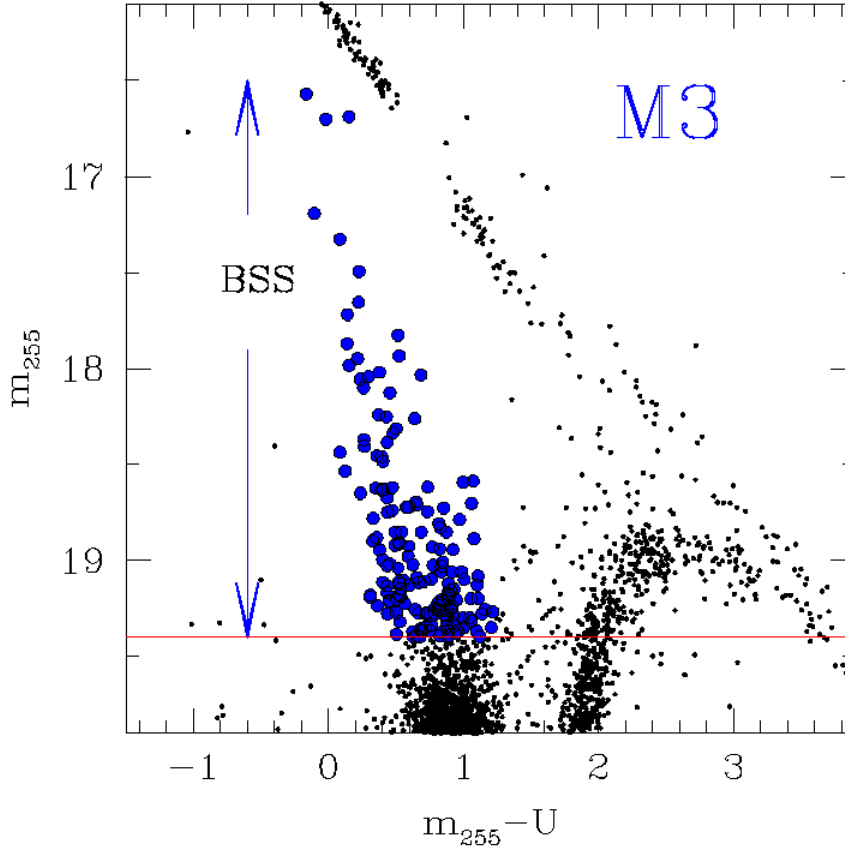


Figure 2. BSS in the UV: the case of M3. The horizontal line at $m_{255} = 19.4$ is the assumed limiting magnitude ($\sim 5\sigma$ above the TO level (from F97)).

2.2. M3: a new approach to study GC stellar populations

M3 has played a fundamental role in the BSS history, since it is the GC where BSS have been identified for the first time, but also the first GC in which the BSS radial distribution has been studied over the entire cluster extension. In fact by combining UV HST observations in the central region of the cluster (F97, see Figure 2) and extensive wide field ground-based observations (F93 - Buonanno et al 1994), F97 presented the radial distribution of BSS over the entire radial extension ($r \sim 6'$).

The UV search for BSS in the central region of M3 led to the discovery of a large population of *centrally segregated* BSS (see Figure 2), contrary to the previous claim by Bolte, Hesser & Stetson (1993) who suggested a possible depletion of BSS in the central region of the cluster with respect to the external regions. As expected, the BSS candidates occupy a narrow, nearly vertical, sequence spanning ~ 3 mag in m_{255} . Two limits (one in color, and one in magnitude) have been assumed to properly select the BSS sample in the UV-CMD shown in Figure 2. The BSS sequence blends smoothly into the MS near the cluster TO. In order to select ‘safe’ BSS, only stars brighter than $m_{255} \sim 19.4$ (0.3 mag brighter than the cluster TO) have been considered.

Beside this, a much more unexpected result was found from the analysis of BSS in M3. In fact, in order to extend the BSS analysis to the whole radial extension of the cluster and to compare the HST sample with the external (ground-based) one, F97 limited the BSS analysis to the brighter portion ($m_{255} < 19$) of BSS population. The radial distribution of the BSS candidates was compared to that of a sample of RGB stars assumed as “reference” population. The cumulative radial distributions of the entire sample split into two sub-sets (at $r = 150''$) are reported in Figure 3: as can be seen the BSS (solid line) are more centrally concentrated than RGB stars (dotted line) in the central regions (out to $r < 150''$), while are less concentrated in the outer ones.

In order to further investigate this surprising result, F97 computed the doubly normalized ratios for the BSS and the RGB stars, following the definitions by F93:

$$R_{\text{BSS}} = \frac{(N_{\text{BSS}}/N_{\text{BSS}}^{\text{tot}})}{(L^{\text{sample}}/L_{\text{tot}}^{\text{sample}})}$$

and

$$R_{\text{RGB}} = \frac{(N_{\text{RGB}}/N_{\text{RGB}}^{\text{tot}})}{(L^{\text{sample}}/L_{\text{tot}}^{\text{sample}})}$$

respectively.

The surveyed cluster region has been divided in a number of concentric annuli and the numbers of BSS and RGB counted in each annulus has been normalized to the sampled luminosity accordingly to the above relations. The *relative frequency* of BSS is compared with that computed for the RGB “reference” stars as a function of the distance from the cluster center, as shown in Figure 4. As can be seen, the radial distribution of BSS is clearly bimodal: it reaches its maximum at the center of the cluster (showing no evidence of a

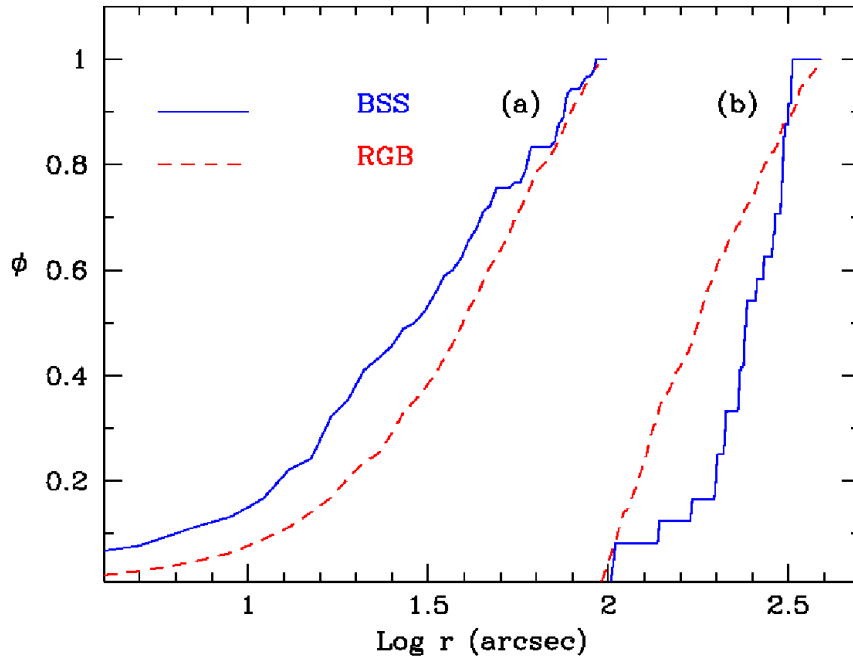


Figure 3. Cumulative distribution of bright BSS (solid lines) in M3 with respect to the RGB (dashed lines), for two radial sub-samples: (a) $r < 2'.5$ and (b) $2'.5 < r < 6'$ (from F97).

BSS depletion in the core); it has a clear-cut dip in the intermediate region (at $100'' < r < 200''$) and a rising trend in the outer region (out to $r \sim 360''$), as first noted by F93.

2.3. 47 Tuc: another surprise!

While the bimodality detected in M3 was considered for years to be *peculiar*, the most recent results demonstrated that this is not the case. In fact, in the last years the same observational strategy adopted by F97 in M3 has been applied to a number of clusters with the aim of determining the BSS frequency over the entire cluster extent. To do this two data-set are generally combined:

(i) *High resolution set*— consisting of a series of high-resolution WFPC2-HST images (typically in the UV) of the cluster center. In this data set the planetary camera (PC, which has the highest resolution $\sim 0''.046/\text{pixel}$) is roughly centered on the cluster center while the Wide Field (WF) cameras (at lower resolution $\sim 0''.1/\text{pixel}$) sample the surrounding outer regions;

(ii) *Wide Field set*— consisting of a series of multi-filter (B , V , I) wide field images obtained by using the last generation of wide field imagers (as for example the Wide Field Imager (WFI) mounted at the 2.2m ESO-MPI telescope

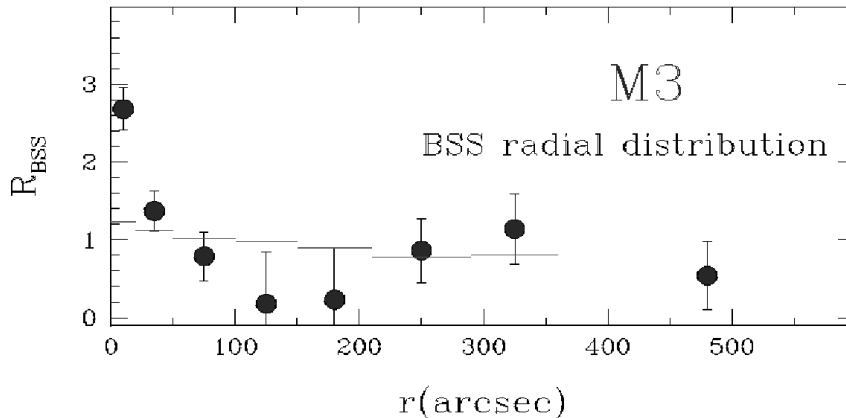


Figure 4. The relative frequency of BSS in M3 is plotted as a function of the radial distance from the cluster center. The horizontal lines show the relative frequency of the RGB stars used as a comparison population. For $r > 6'$ only the relative frequency of BSS has been computed using the Sandage (1953) candidates. (From F97)

at ESO (La Silla)). The WFI is a mosaic of 8 CCD chips (each one with a field of view of $8' \times 16'$) giving a global coverage of $33' \times 34'$.

Figure 5 shows the typical cluster coverage adopting this observing strategy, also used for 47 Tuc (see Ferraro et al 2001a and Ferraro et al 2004a, hereafter F04). Figure 6 shows the corresponding CMD. As can be seen a well defined sequence of BSS has been obtained in both samples. To study the BSS radial distribution, F04 applied the procedure described in F93 (used also in F97) where the surveyed area has been divided into a set of concentric annuli. 11 concentric annuli, each one containing roughly $\sim 10\%$ of the reference population) have been defined in the case of 47 Tuc. The BSS specific frequency has been computed in two different ways: (1) the ratio $F_{\text{BSS}}^{\text{HB}} = N_{\text{BSS}}/N_{\text{HB}}$ and (2) the double-normalized ratio R (see above) considering the fraction of luminosity sampled in each annulus.

Figure 7 shows the distribution of both ratios as a function of the effective radius of each annulus. The distribution is clearly bimodal, with the highest value in the innermost annulus where the $F_{\text{BSS}}^{\text{HB}}$ ratio reaches ~ 0.4 , it significantly decreases to less than 0.1 as r increases and then slowly rises up to ~ 0.3 in the outer region.

This trend is fully confirmed by using the *relative BSS frequency* R_{BSS} (see F97 and above). The behavior of this ratio as a function of the distance from the cluster center is shown in Figure 7 (*panel (b)*) and compared with the corresponding one for the HB “reference” stars. As can be seen, the HB specific frequency remains essentially constant over the surveyed area since the fraction of HB stars (as any post-main sequence stage) in each annulus strictly depends on the fraction of luminosity sampled in that annulus (see the relation by Renzini & Buzzoni 1986, eq 2 in F03). In contrast, the BSS specific frequency reaches its maximum at the center of the cluster, then decreases to an approximately

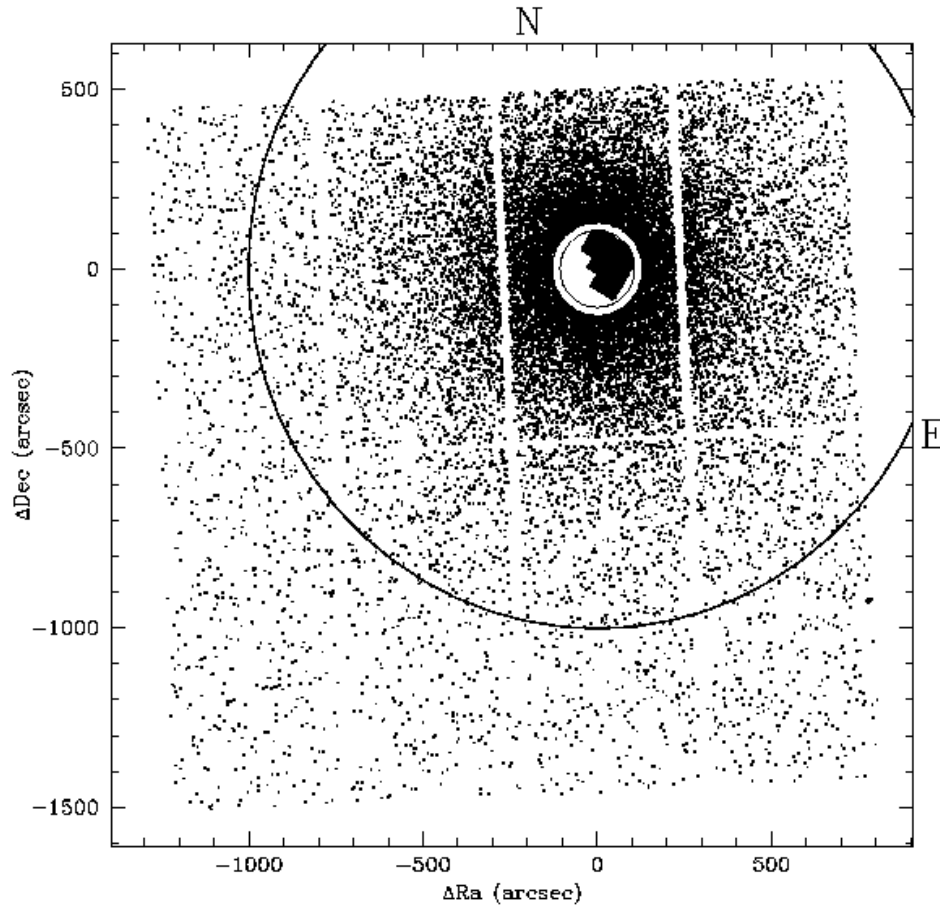


Figure 5. The map shows the observational strategy adopted to study the radial distribution of the BSS frequency in clusters. Typically the central regions are imaged by UV-HST observations, while the external regions are sampled by ground-based wide-field observations (using the Wide Field Imager (WFI) at the 2.2m ESO telescope). Here the case of NGC6752 is shown. (From Sabbi et al 2004).

constant value in the range $100''$ – $500''$ from the cluster center and then rises again. *The trend found in 47 Tuc closely resembles that discovered in M3 by F97.*

To further demonstrate the similarity with M3 and to study possible differences we show the BSS specific frequencies for the two clusters on the same figure (see Figure 8). The radial coordinate is given in units of the core radius r_c , adopting $r_c = 21''$ and $r_c = 24''$ for 47 Tuc and M3, respectively (see F04 and F03). A few major characteristics about Figure 8 are worth noticing: (1) the central values are similar; (2) while the BSS specific frequency decreases in both clusters as r increases from 0 to $\sim 4r_c$, the decrease is much larger in M3. In 47 Tuc it is a factor of 5.5, dropping from 2.64 down to 0.48; in M3 the

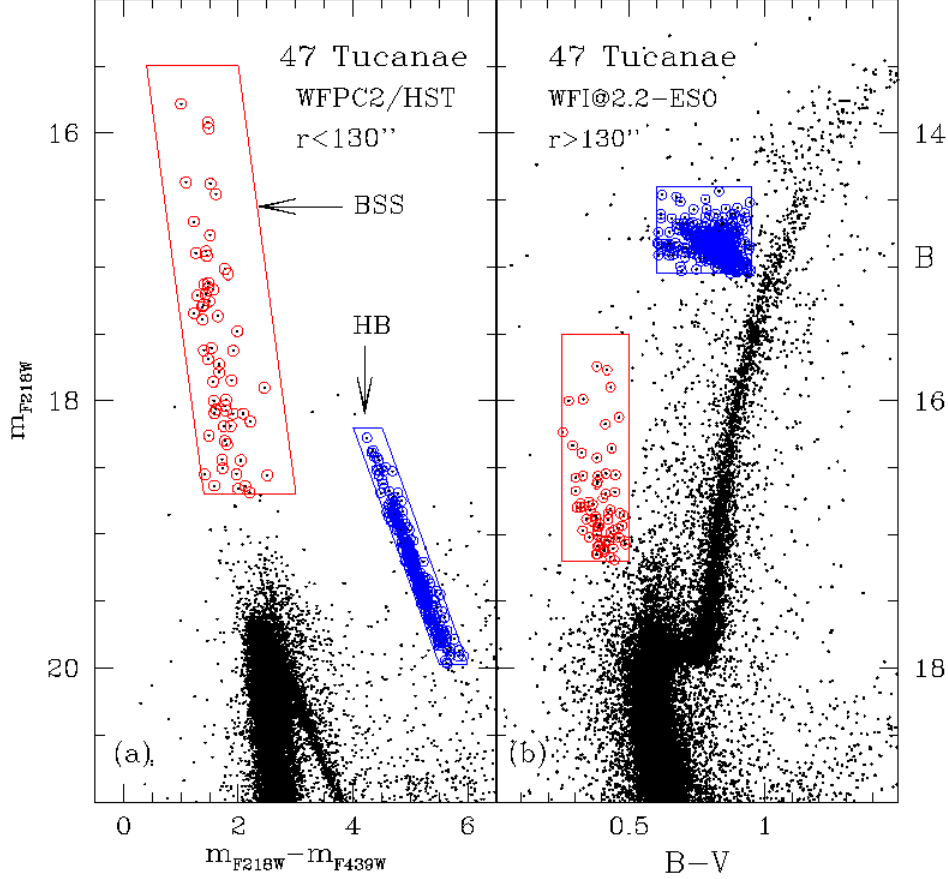


Figure 6. *Panel (a)*: $(m_{218}, m_{218} - m_{439})$ CMD of the central region of 47 Tuc ($r < 130''$) from WFPC2/HST observations. *Panel (b)*: $(B, B - V)$ CMD for the external part of 47 Tuc ($130'' < r < 1500''$) from ground-based observations. The two selection boxes for the BSS and the reference HB population are shown. (From Ferraro et al 2001a and F04).

drop is a factor of 15 (from 2.76 to 0.2). (3) the specific frequency minimum in 47 Tuc appears to be much broader than that observed in M3. In 47 Tuc the depletion zone extends from $\sim 4r_c$ to $20\text{--}22 r_c$ with the upturn of the BSS density occurring at $\sim 25 r_c$, while in M3 the BSS specific frequency is already rising at $\sim 8r_c$.

F97 argued that the bimodal distribution of BSS in M3 was a signature that two formation scenarios were active in the same cluster, the *external* BSS arising from mass transfer in primordial binaries and the *central* BSS arising from stellar interactions which lead to mergers. As earlier noted by Bailyn & Pinsonneault (1995), the luminosity functions of the two BSS samples differ as theoretically expected for the two different mechanisms.

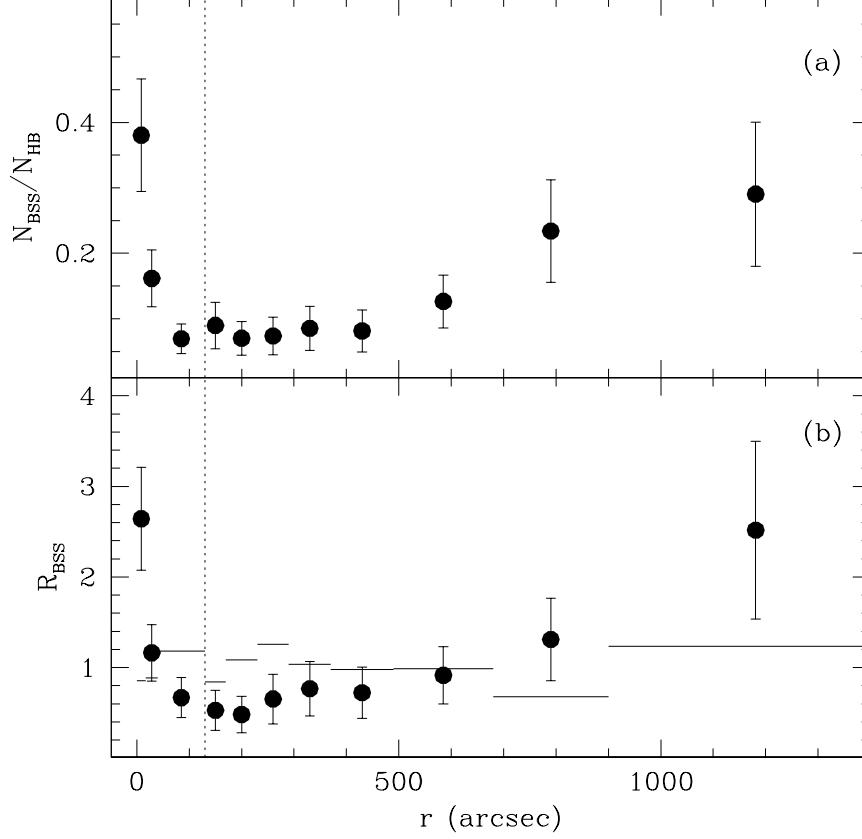


Figure 7. *Panel (a)*: The relative frequency of BSS with respect to HB stars is plotted as a function of the distance from the cluster center. *Panel (b)*: The specific frequency of BSS is plotted. The horizontal lines show the specific frequency for the HB reference population. The vertical dotted line separates the cluster regions observed with HST from those observed from the ground. (From F04).

Sigurdsson et al. (1994) offered another explanation for the bimodal BSS distribution in M3. They suggested that the *external* BSS were formed in the core and then ejected into the outer regions by the recoil from the interactions. Those binaries which get kicked out to a few core radii (r_c) rapidly drift back to the center of the cluster due to mass segregation, leading to a concentration of BSS near the center and a paucity of BSS in the outer parts of this region. More energetic kicks will take the BSS to larger distances; these stars require much more time to drift back toward the core and may account for the overabundance of BSS at large distances. In order to discern between different possibilities accurate simulations with suitable dynamical codes are necessary. Mapelli et al (2004) modeled the evolution of BSS in 47 Tuc, mimicking their dynamics in a

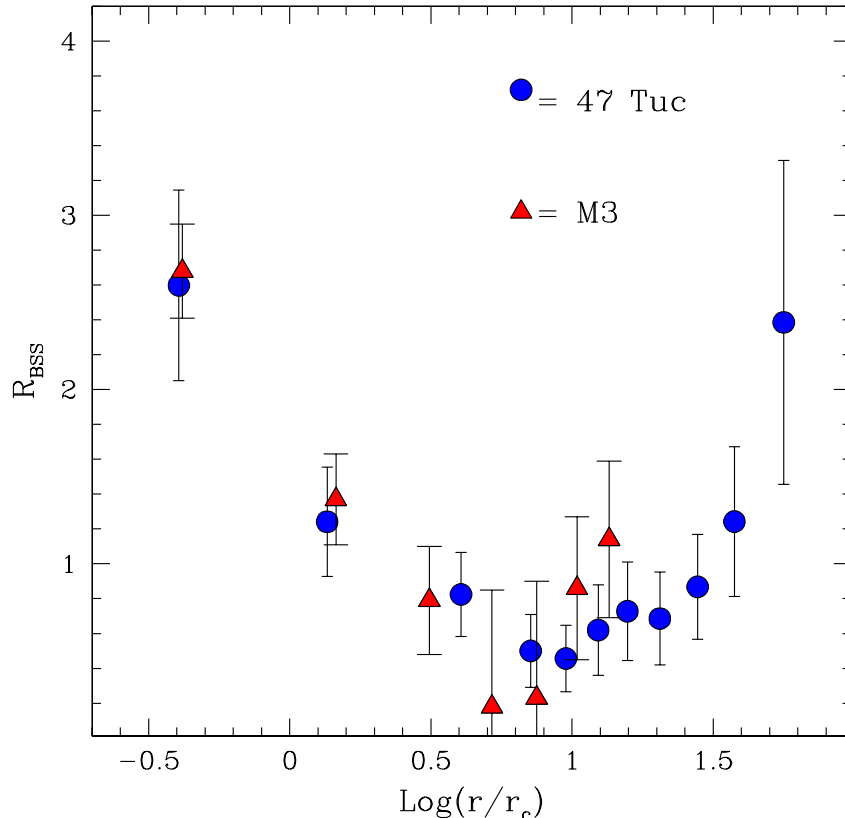


Figure 8. The specific frequency of BSS in 47 Tuc (filled circles) is compared with that found in M3 (filled triangles). The radial coordinate is expressed in unit of core radii r_c . (From F04).

multimass King model, by using a new version of the dynamical code described by Sigurdsson & Phinney (1995). Their results demonstrate that the observed spatial distribution cannot be explained within a purely collisional scenario in which BSS are generated exclusively in the core through stellar interactions. In fact, an accurate reproduction of the BSS radial distribution can be obtained only requiring that a sizable fraction of BSS is generated in the peripheral regions of the cluster inside primordial binaries that evolve in isolation and experiencing mass transfer.

A BSS specific upturn similar to that observed in 47 Tuc and M3 has also been detected in M55 by Zaggia et al. (1997). This result is based on ground-based observations sampling only a quadrant of the cluster. Since ground-based observations tend to hide BSS in the central region of the cluster, the bimodality in M55 could be even stronger than that found by Zaggia et al (1997). This is of particular significance because M55 has a central density significantly lower

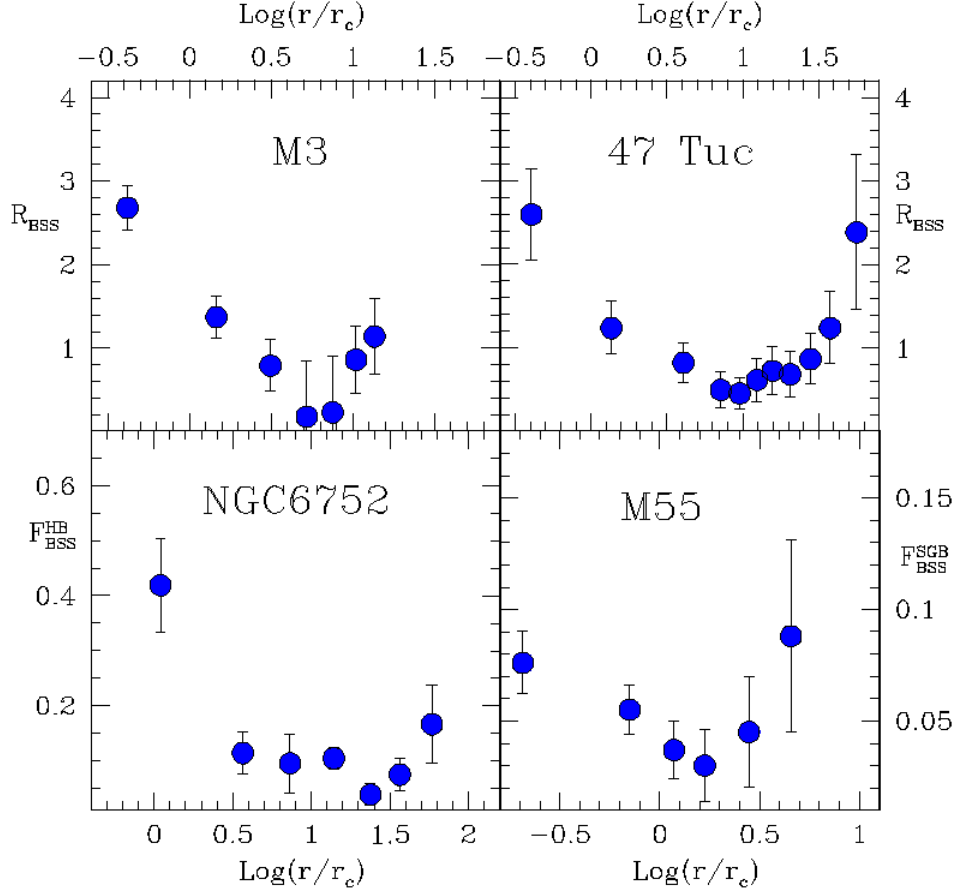


Figure 9. The bimodal distribution of BSS discovered in GCs up to now.

than M3 and 47 Tuc and could suggest that the bimodal distribution is not related to the central density of the parent cluster. Moreover a BSS bimodal radial distribution has been also recently detected in NGC6752 by Sabbi et al (2004). At present, there are at least 4 GCs in which the BSS radial distribution seems to be bimodal: M3, 47 Tuc, M55 and NGC6752 (see Figure 9).

Though the number of the surveyed clusters is low, these discoveries suggest that the *peculiar* radial distribution first found in M3 is much more *common* than was thought. *Indeed, it could be the “natural” BSS radial distribution.* Clearly, generalizations cannot be made from a sample of a few clusters. Hence we need to characterize the BSS radial distribution on a much more solid statistical base. First results from simulations indicate that bimodality is a signature that both collisions and primordial binaries play an important role.

However, there is recent evidence that BSS do not follow this rule in at least one cluster. Using combined (HST+ground-based) observations Ferraro et al (2005) selected the largest population of BSS ever observed in a stellar

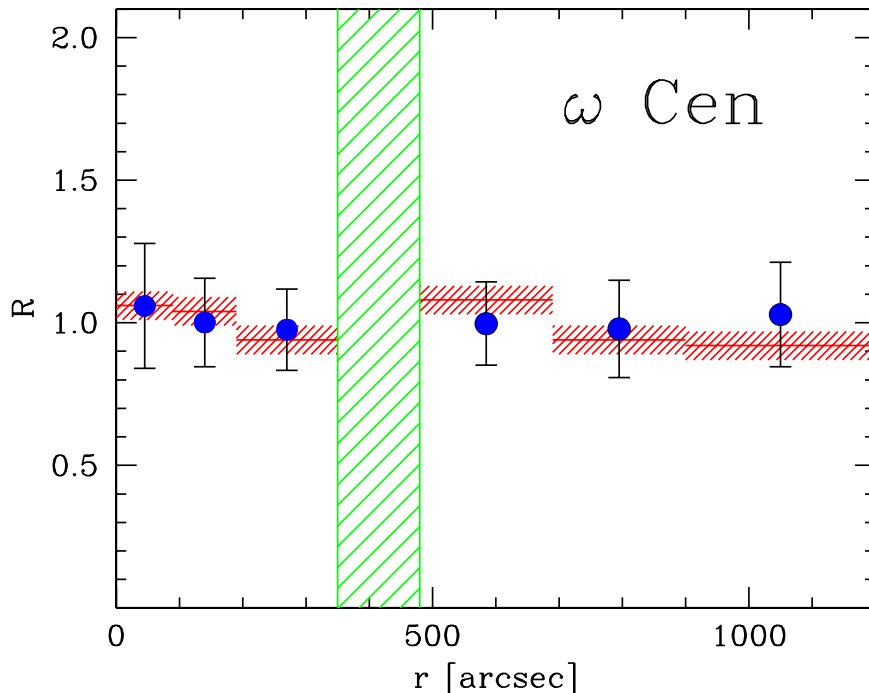


Figure 10. The double-normalized relative frequency R_{BSS} of the BSS (filled circles) in ω Cen. The shaded area marks the cluster region we excluded in order to avoid incompleteness problems. The horizontal lines show the relative frequency of the RGB stars used as reference population. (From Ferraro et al 2005).

system in the giant cluster ω Cen. Conversely to any other GC surveyed up to now, they found that the BSS frequency in this stellar system *does not peak in the center and does not vary with the distance from the cluster center*. As can be seen from Figure 10, the double normalized BSS ratio turns out to be nicely constant over the entire cluster extension and it is fully consistent with the reference population. This is the very first time that such a trend has been found for BSS. This result is surprising since the relaxation time for the core of the cluster ($\tau \sim 7$ Gyr) is a factor two lower than the estimated cluster age ($t \sim 13$ Gyr). Clearly this evidence could be related to the complex history of this peculiar stellar system (see recent results in Lee et al 1999; Pancino et al 2000, 2002; Ferraro et al 2002, 2004b). *However, our observations give the cleanest evidence that this cluster has not yet reached the energy equipartition*

even in the central core and further support the use of BSS as probe of the dynamical cluster evolution.

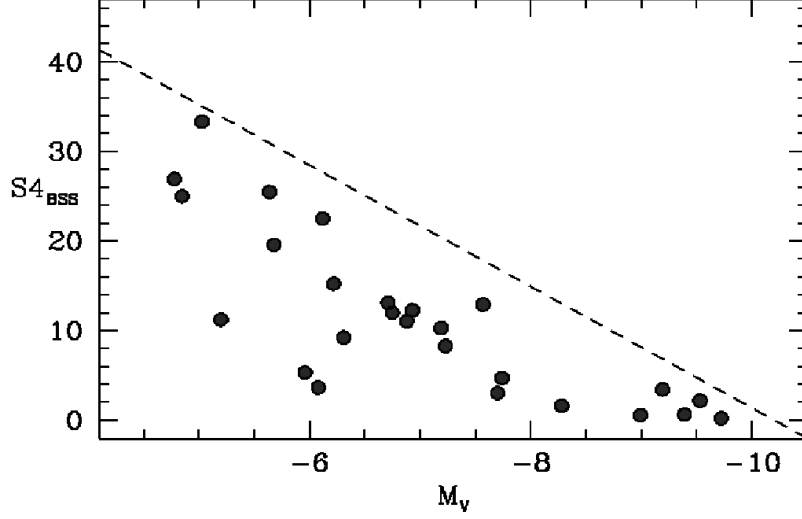


Figure 11. BSS relative frequency ($S4_{BSS}$) as a function of the cluster integrated absolute magnitude. (From FFB95).

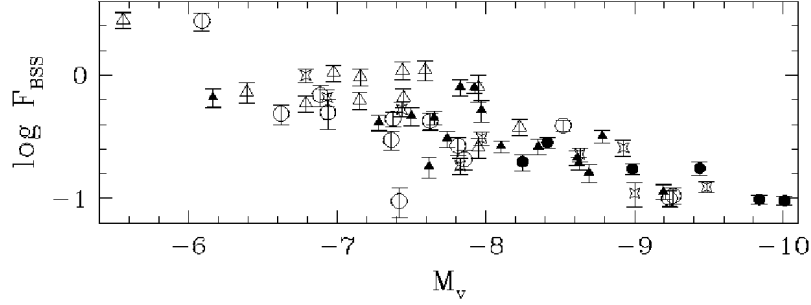


Figure 12. BSS relative frequency (F_{BSS}) as a function of the cluster integrated absolute magnitude: different symbols are used for clusters with different central densities. (From Piotto et al 2004).

2.4. BSS and the parent GC properties

Specific BSS frequencies and structural parameters The collection of an homogeneous dataset of BSS in different clusters allows a direct cluster-to-cluster comparison. However, it should be emphasized that the interpretation of BSS specific frequency in terms of structural cluster parameters can be risky (see FFB95). In particular, one should keep in mind the intrinsic dependence of any BSS specific frequency on the cluster luminosity.

Recently, Piotto et al. (2004) noted a correlation between BSS specific frequency and cluster absolute magnitude. The same correlation had been discussed by FFB95 (see Fig. 11 and 12), who showed that much of this effect arose from the normalization of the population. Indeed such a trend could be generated by the correlation between the sampled and the total luminosity as shown in Fig. 4 of FFB95. A similar analysis should be performed on the Piotto et al (2004) sample in order to establish the role of the normalization factor in defining the observed trend.

Based on the results of Piotto et al., Davies et al. (2004) developed a model for the production of BSS in GGCs. In the low mass systems ($M_V > -8$) BSS arise mostly from mass exchange in primordial binaries. In more massive systems collisions produce mergers of the primordial binaries early in the cluster history. BSS resulting from these mergers long ago evolved away. Once the primordial binaries were used up, BSS produced via this channel disappeared. In the cores of the most massive systems ($M_V < -9$) collisional BSS are produced (see Fig. 6 of Davies et al.). The working hypothesis proposed by Davies et al (2004) is interesting, however detailed cluster-to-cluster comparison has shown that the scenario is much more complex than that, since the dynamical history of each cluster apparently plays a significant role in determining the origin and radial distribution BSS content (see next Section).

Cluster to cluster comparison In the contest of a direct comparison of the BSS content in different clusters, particularly interesting is the case of M80, which shows an exceptionally high BSS content: more than 300 BSS have been discovered (Ferraro et al 1999). This is among the largest and most concentrated BSS population ever found in a GGC (see Figure 13). Indeed only the largest stellar system in the Halo, ω Centauri, has been found to harbor a BSS population (Ferraro et al 2005) larger than that discovered in M80. M80 is the GGC which has the largest central density among those not core-collapsed yet. However, the stellar density cannot explain such a large population, since other clusters with similar central density harbor much fewer BSS (see the case of 47 Tuc, Ferraro et al 2001a, NGC6388 Piotto et al 2003). Ferraro et al (1999) suggested that M80 is in a transient dynamical state during which stellar interactions are delaying the core-collapse process, leading to an exceptionally large population of collisional BSS. If this hypothesis would be further confirmed, this discovery could be the first direct evidence that stellar collisions could indeed be effective in delaying the core collapse.

Interesting enough, clusters that have already experienced (or are experiencing) the collapse of the core show a small BSS population. Indeed this is the case of NGC6752. This cluster has been recently found (see Ferraro et al 2003d) to be dynamically evolved probably undergoing a Post Core Collapse bounce (see Section 3.4). A recent search for BSS in the central region of this cluster indicated a surprisingly low BSS content: the specific number of BSS is among the lowest ever measured in a GC (Sabbi et al 2004, see Figure 14).

F03 presented a direct comparison of the BSS content for 6 clusters observed in the UV with HST (namely M3, M13, M80, NGC288, M92 and M10). Figure 15 shows the (m_{255} , $m_{255} - m_{336}$) CMDs for these clusters. More than 50,000 stars are plotted in the six panels of Figure 15. The CMD of each cluster has been shifted to match that of M3 using the brightest portion of the HB as the

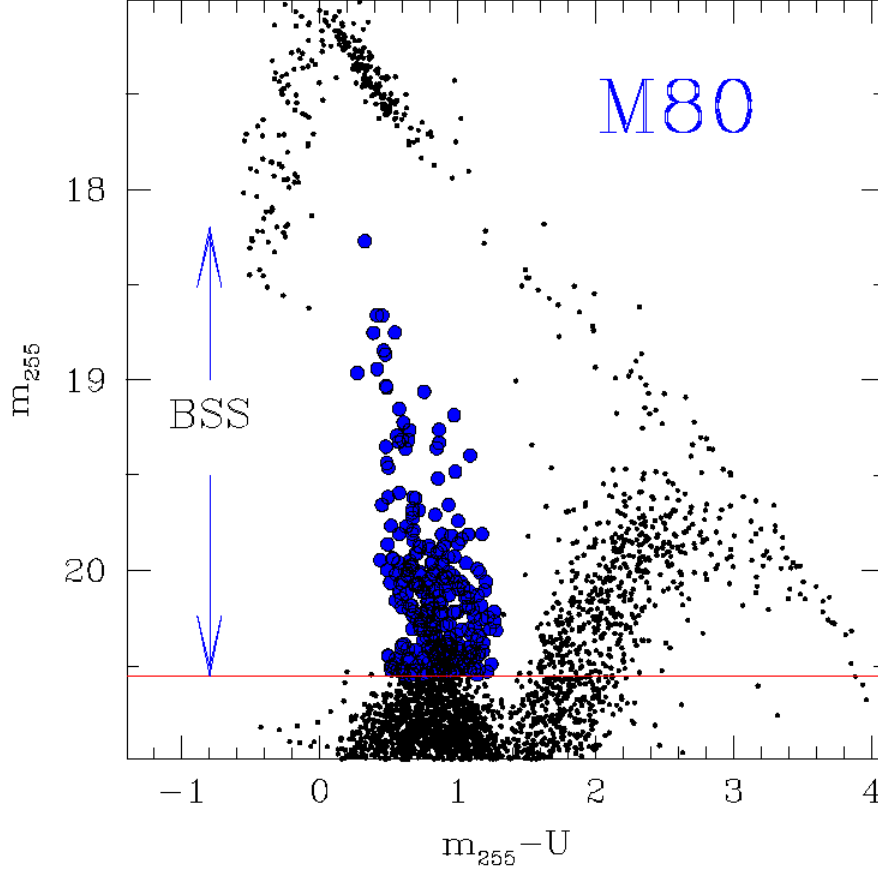


Figure 13. $(m_{255}, m_{255}-m_{336})$ CMD for the central region of M80, from WFPC2/HST observations. The 300 BSS candidates discovered in this cluster are marked as filled circles. (From Ferraro et al 1999).

normalization region. The solid horizontal line (at $m_{255} = 19$) in the figure marks the threshold magnitude for the selection of the bright (hereafter bBSS) sample. Such a dataset allows a direct cluster-to-cluster comparison. A number of interesting results have been obtained and in the following we just briefly discuss the two major ones:

- the specific frequency of BSS largely varies from cluster to cluster. The specific frequency of BSS compared to the number of HB stars varies from 0.07 to 0.92 for these six clusters, and does not seem to be correlated with central density, total mass, velocity dispersion, or any other obvious cluster property. Twins clusters as M3 and M13 harbor a quite different BSS population: the specific frequency in M13 is the lowest ever measured in a GC (0.07), and it turns out to be 4 times lower than that measured in M3 (0.28). Which is the origin of this difference? The paucity of BSS

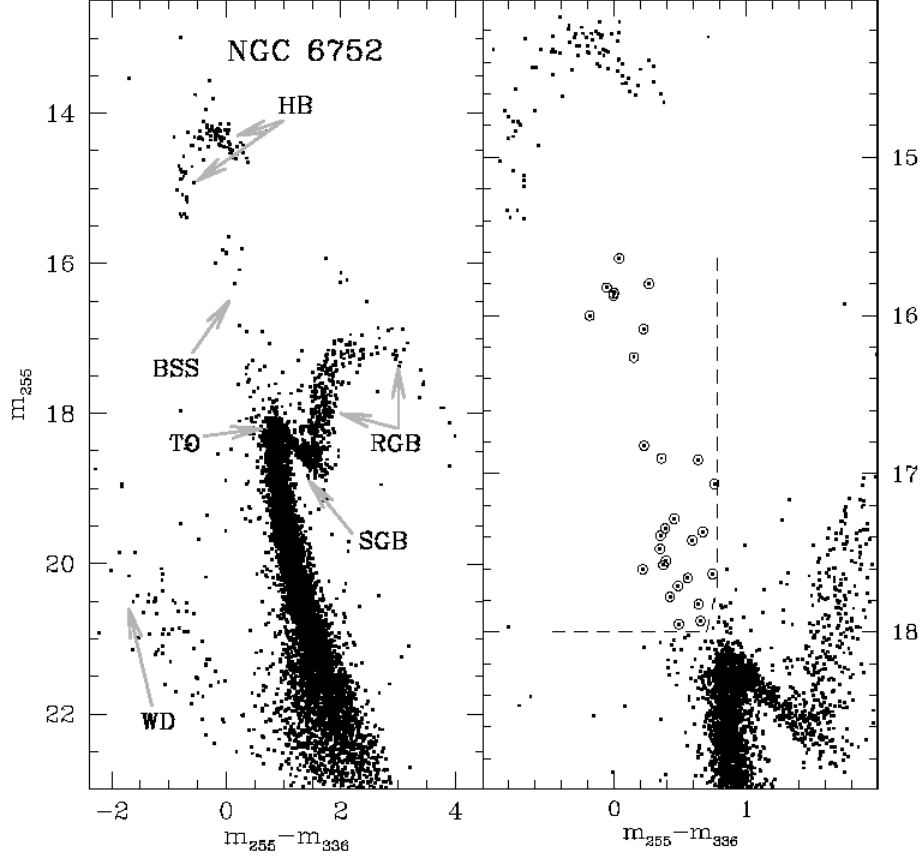


Figure 14. $(m_{255}, m_{255}-m_{336})$ CMD for the central region of NGC 6752, from WFPC2/HST observations. *Left panel:* The whole CMD. The main branches are indicated. *Right panel:* The zoomed CMD in the BSS region. The selected BSS are marked with large empty circles. (From Sabbi et al 2004).

in M13 suggests that either the primordial population of binaries in M13 was poor or that most of them were destroyed. Alternatively, as suggested by F97, the mechanism producing BSS in the central region of M3 is more efficient than M13 because M3 and M13 are in different dynamical evolutionary phases.

In this respect, the most surprising result is that the two clusters with the largest BSS specific frequency are at the central density extremes of our sample: NGC 288 (lowest central density) and M80 (highest). The BSS specific frequency measured in these clusters (Bellazzini et al 2002, and Ferraro et al 1999) suggest that both of them have almost as many BSS as HB stars in the central region. F03 have shown that the collision channel is more than one order of magnitude more efficient in a dense

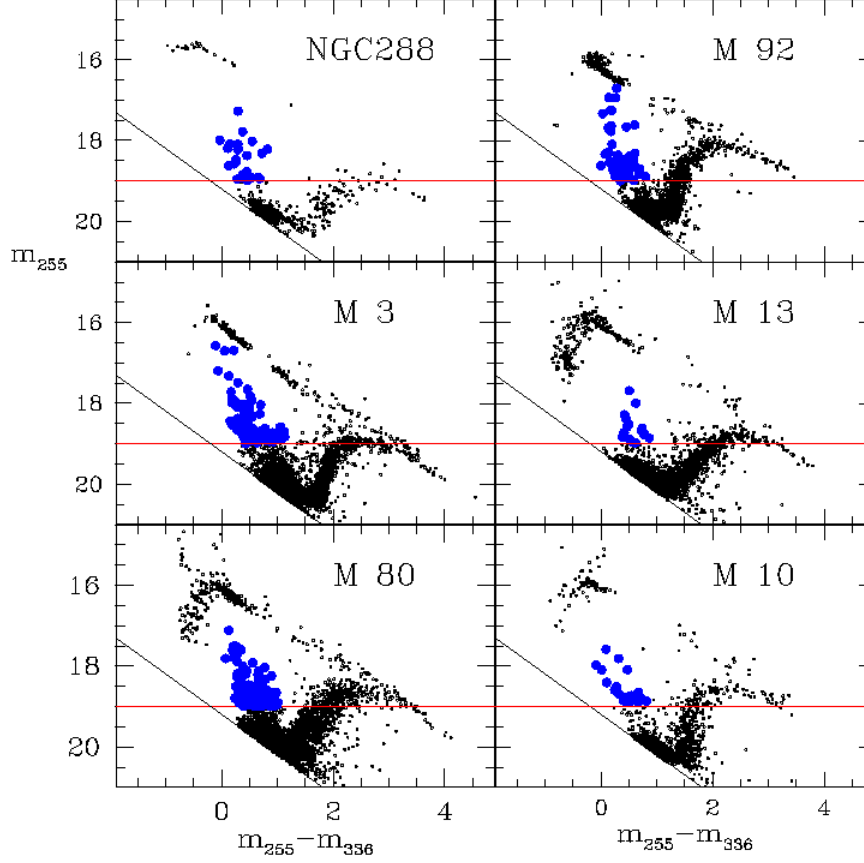


Figure 15. $(m_{255}, m_{255} - m_{336})$ CMDs for the selected clusters. Horizontal and vertical shifts have been applied to all CMDs in order to match the main sequences of M3. The horizontal solid line corresponds to $m_{255} = 19$ in M3. The bright BSS candidates are marked as large filled circles. (From F03).

cluster like M80 than in a low density cluster like NGC 288. Therefore, the high specific frequency of BSS in NGC 288 suggests that the binary fraction in this cluster is much higher than the one in M80. Only then would one expect a similar encounter frequency in the two clusters. Note that a cluster like M80 may have originally had a higher binary fraction but because of the efficiency of encounters, those primordial binaries were “used up” early in the history of the cluster, producing some collisional BSS which have evolved away from the MS (see for example the evolved BSS population found in M3 and M80 by F97 and Ferraro et al. (1999, see also Section 2.6).

However, without invoking *ad hoc* binary content, a *more natural explanation* for the origin of BSS in NGC 288 (as discussed in Bellazzini et al (2002)) is the mass transfer process in primordial binary systems (Carney

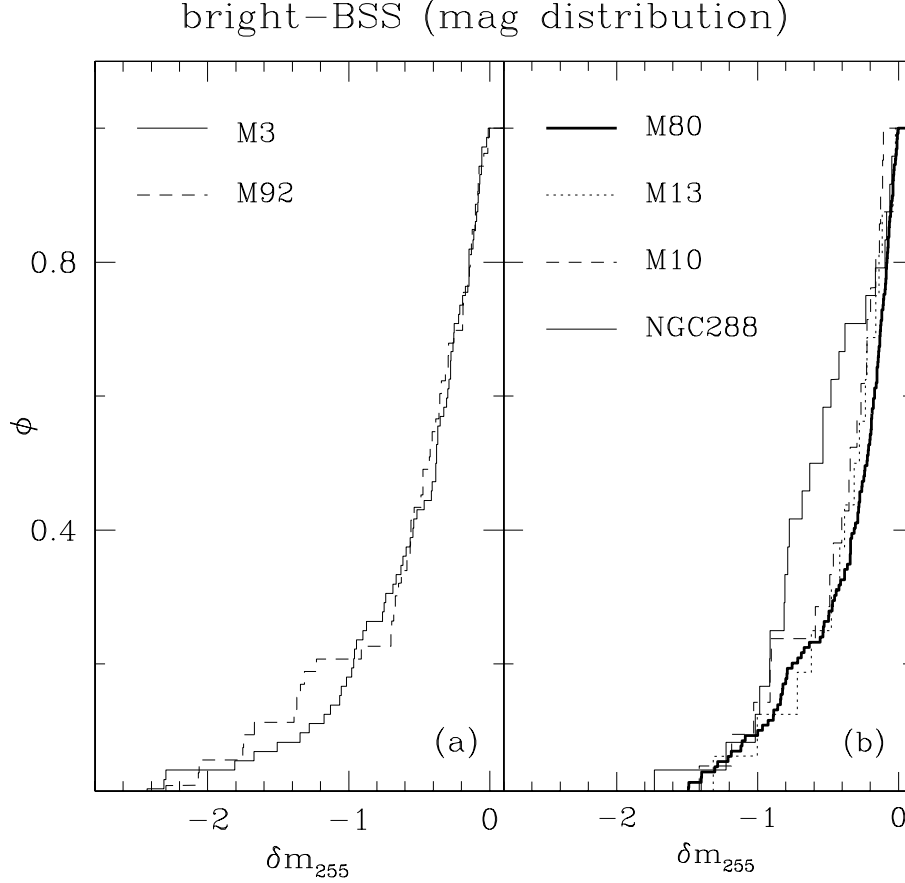


Figure 16. Cumulative magnitude distributions for the *bright* BSS for the 6 clusters presented by F03. The δm_{255} parameter is the difference in magnitude with respect to the limit threshold ($m_{255} = 19$) for bright-BSS. In *Panel (a)* the BSS distributions for M3 and M92 (the two clusters for which the BSS distribution extends up to more than two magnitudes brighter than the threshold) are compared. In *Panel (b)* the BSS magnitude distributions for the other 4 clusters are plotted. (From F03).

et al 2001). We also know that the binary fraction in the core is ~ 10 to 38% (Bellazzini et al 2002), so BSS formed in this low density cluster should be the result of binary evolution rather than stellar collisions. Here we probably have another confirmation of the scenario suggested by Fusi Pecci et al (1992, and references therein): BSS living in different environments have different origins. In this case the above result demonstrated that both channels are quite efficient in producing BSS.

- In Figure 16 the magnitude distributions (equivalent to a Luminosity Function) of bBSS for the six clusters are compared. In doing this we use the parameter δm_{255} defined as the magnitude of each bBSS with respect to

the magnitude threshold (assumed at $m_{255} = 19$ - see Figure 15): then $\delta m_{255} = m_{255}^{bBSS} - 19.0$. From the comparison shown in Figure 16 (*panel(a)*) the bBSS magnitude distributions for M3 and M92 appear to be quite similar and both are significantly different from those obtained in the other clusters. This is essentially because in both clusters the bBSS magnitude distribution seems to have a tail extending to brighter magnitudes (the bBSS magnitude tip reaches $\delta m_{255} \sim -2.5$). A KS test applied to these two distributions yields a probability of 93% that they are extracted from the same distribution. In *panel(b)* we see that the bBSS magnitude distribution of M13, M10 and M80 are essentially indistinguishable from each other and significantly different from M3 and M92. A KS test applied to the three LFs confirms that they are extracted from the same parent distribution. Moreover, a KS test applied to the total LFs obtained by combining the data for the two groups: M3 and M92 (*group(a)*), and M13, M80 and M10 (*group(b)*) shows that the the bBSS-LFs of *group(a)* and *group(b)* are not compatible (at 3σ level).

It is interesting to note that the clusters grouped on the basis of bBSS-LFs have some similarities in their HB morphology. The three clusters of *group(b)* have an extended HB blue tail; the two clusters of *group(a)* have no HB extension. Could there be a connection between the bBSS photometric properties and the HB morphology? This possibility needs to be further investigated.

2.5. Comparison with collisional models

A preliminary comparison between the observed BSS distribution in the CMD (and their LF) with those obtained from collisional models have been presented in F03. The models used there are described in detail in Sills & Bailyn (1999). The main assumption is that all the BSS in the central regions are *formed through stellar collisions during an encounter between a single star and a binary system*. Unfortunately, while binary-binary collisions may well be important, we do not currently have the capability of modeling the BSS they might produce.

The other ingredients of the collisional models are discussed in F03, in the following we list the major assumptions:

- The trajectories of the stars during the collision are modeled using the STARLAB software package (McMillan & Hut 1996).
- The adopted mass function has an index $x = -2$, and the mass distribution within the binary systems are drawn from a Salpeter mass function ($x = 1.35$).
- The adopted binary fraction is 20% with a binary period distribution which is flat in $\log P$.
- The total stellar density is derived from the central density of each cluster.

In order to explore the effects of non-constant BSS formation rates, we considered a series of truncated rates, namely constant for some portions of the

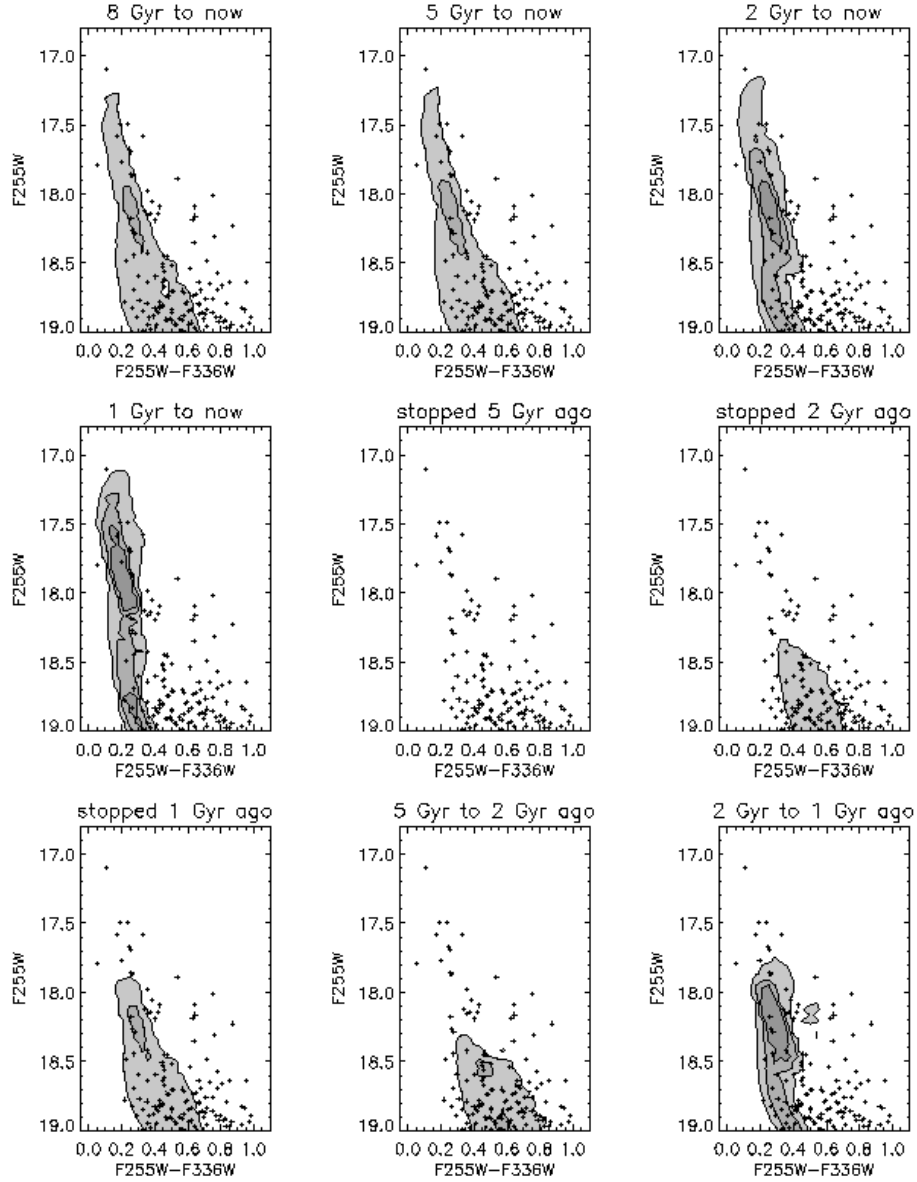


Figure 17. The distribution of bright BSS in the CMD of M80, compared to theoretical distributions. The observations are plotted as crosses, and the grey scale contours give the theoretical distributions, with darker colors indicating more BSS. The different panels correspond to different eras of constant BSS formation, as indicated at the top of each panel. (From F03).

cluster lifetime, and zero otherwise. This assumption is obviously unphysical—the relevant encounter rates would presumably change smoothly on timescales comparable to the relaxation time. However these models do demonstrate how the distribution of BSS in the CMD depends on when the BSS were created, and

thus provide a basis for understanding more complicated and realistic formation rates.

Figure 17 shows an example of the distribution of BSS in the m_{255} , $m_{255} - m_{336}$ CMD as predicted by collisional models in the case of M80. In each panel, a different assumption for the BSS formation rate has been adopted. The differences between the models can be understood in terms of lifetimes of the individual collision products which make up the distributions. For example, if BSS production stopped 5 Gyr ago (central panel), we predict that there should be no observed bBSS at present because all the massive BSS had time to evolve off to the RGB. At the other extreme, if all the BSS were formed in the last Gyr (panel marked “1 Gyr to now”), only a few (if any) of the brightest (i.e. most massive) BSS started moving towards the subgiant branch.

As a general result, F03 concluded that the BSS formation occurred in all clusters over last 5 Gyr at least, and more were formed 2–5 Gyr ago than in the recent past. Of course this result needs to be tested using models of GC dynamical evolution in which the feedback between stellar collisions and cluster evolution is modeled explicitly. Our assumption of a BSS formation rate which is either constant or zero is unphysical, and more complicated models are clearly required.

2.6. Evolved BSS on the HB

Renzini & Fusi Pecci (1988) suggested to search for Evolved BSS (hereafter E-BSS) during their core helium burning phase since they should appear to be redder and brighter than *normal* HB stars. Following this prescription, Fusi Pecci et al. (1992) identified a few E-BSS candidates in several clusters with predominantly blue HBs, where the likelihood of confusing E-BSS stars with true HB or evolved HB stars was minimized. Because of the small numbers there is always the possibility that some or even most of these candidate E-BSS are due to field contamination. However, near the cluster centers, field contamination should be less of a problem. Following Fusi Pecci et al (1992), F97 identified a sample of 19 E-BSS candidates in M3 (see Figure 18) and argued that the radial distribution of E-BSS was similar to that of the BSS.

The large population of BSS discovered by Ferraro et al (1999) in M80 allowed a further possibility to search for E-BSS, in fact, M80 offers some advantages over M3 in selecting E-BSS: (1) it has a very blue HB, so there should be less confusion between red HB stars and E-BSS; (2) it has a larger number of BSS. In Figure 19 *Panel (a)* a zoomed (U , $U - V$) CMD of the HB region is shown and the expected location for E-BSS has been indicated as a box; 19 E-BSS (plotted as large filled circles) lie in the box. The cumulative radial distribution of the E-BSS stars shown in *Panel (b)* of Figure 19 is quite similar to the BSS distribution and significantly different from that of the HB-RGB. A Kolmogorov-Smirnov test shows that the probability that the E-BSS and BSS populations have been extracted from the same distribution is $\sim 67\%$, while the probability that the E-BSS and the RGB-HB population have the same distribution is only $\sim 1.6\%$. This result confirms the expectation that the E-BSS share the same distribution of the BSS and they are both a more massive population than the bulk of the cluster stars.

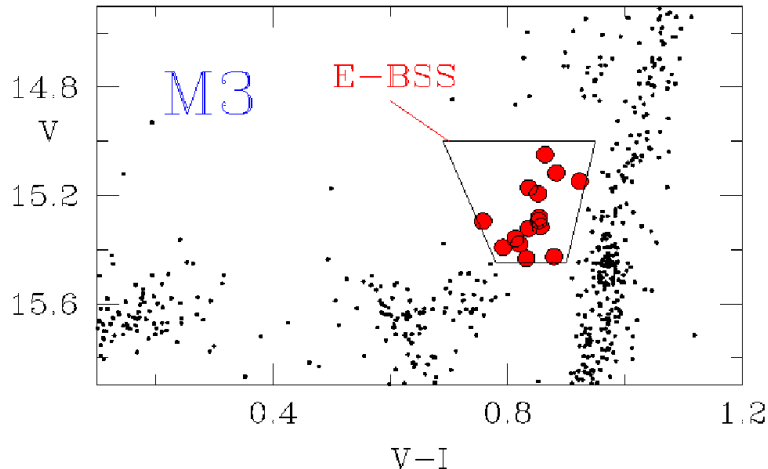


Figure 18. Zoomed $(V, V - I)$ -CMD of the HB region of M3. Evolved BSS candidates are plotted as large filled circles. (From F97).

Under the assumption that the connection between the E-BSS and the BSS population is real, one can relate the population ratios and the lifetimes of these evolutionary stages. Earlier studies (Fusi Pecci et al 1992) have suggested that the ratio of bright BSS (b-BSS) to E-BSS is $N_{\text{b-BSS}}/N_{\text{E-BSS}} \approx 6.5$. Interesting enough, the population ratios are quite similar in both clusters: in M3 F97 counted 19 E-BSS over a population of 122 bBSS; the same number of E-BSS candidates have been selected by Ferraro et al (1999) in M80 compared with a population of 129 b-BSS. The population ratio turns out to be $N_{\text{b-BSS}}/N_{\text{E-BSS}} = 6.6$, fully consistent with earlier studies. Moreover because both BSS and E-BSS samples are so cleanly defined in the case of M80, the ratio of the total number of BSS to E-BSS, $N_{\text{BSS}}/N_{\text{E-BSS}} \sim 16$, should be useful in testing lifetimes of BSS models.

3. MSP companions in GCs

Among the possible collisional by-product zoo, MSPs are invaluable probes to study cluster dynamics: they form in binary systems containing a neutron star (NS) which is eventually spun up through mass accretion from the evolving companion. Despite the large difference in total mass between the disk of the Galaxy and the GC system, about 50% of the entire MSP population has been found in the latter. This is not surprising since in the Galactic disk MSPs can only form through the evolution of primordial binaries, while in GC cores dynamical interactions can lead to the formation of several different binary systems, suitable for recycling NS.

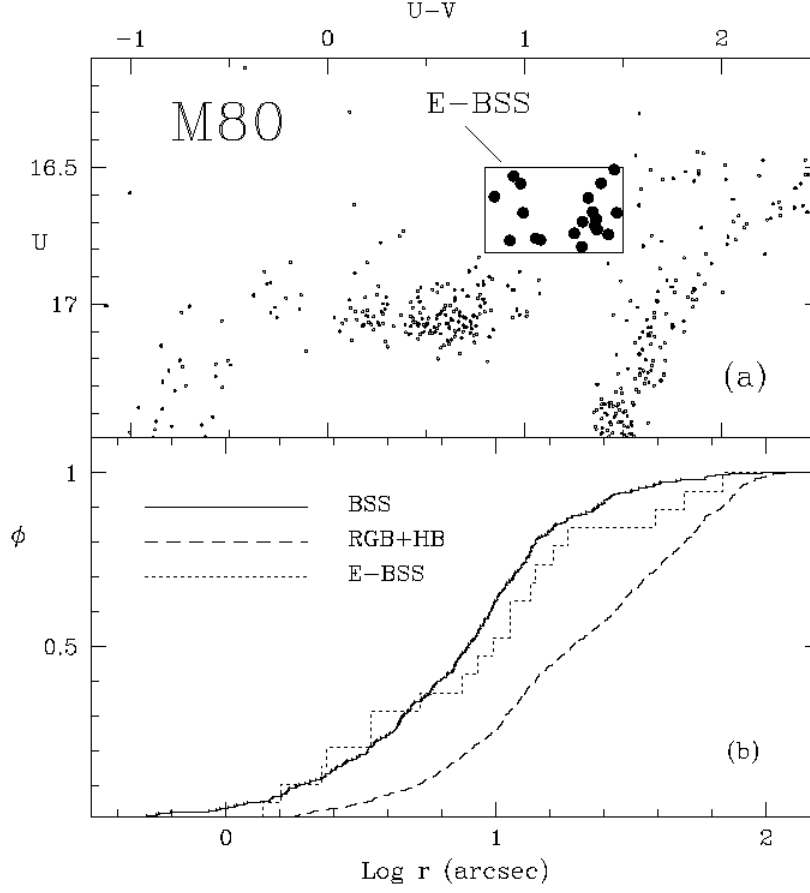


Figure 19. *Panel (a)* Zoomed $(U, U - V)$ CMD of the HB region of M80. Evolved BSS (E-BSS) candidates are plotted as large filled circles. *Panel (b)* Cumulative radial distribution (ϕ) for BSS (heavy solid line), E-BSS (dotted line) compared to the HB+RGB stars (dashed line) as a function of their projected distance (r) from the cluster center. (From Ferraro et al 1999).

The search for optical counterpart to MSP companion in GCs is a relatively recent branch of this research, since the first identification has been done only a few years ago in the core of 47 Tuc. Edmonds et al (2001) identified U_{opt} , the companion to PSR J0024–7203U: this object turned out to be a faint blue variable whose position in the CMD is consistent a cooling helium WD. This is fully in agreement with the MSP recycling scenario, where the usual companion to a binary MSP is an exhausted star.

3.1. The surprising companion to the MSP in NGC6397

A major surprise came from the optical identification of the companion to the binary MSP PSR J1740-5340 in NGC6397.

PSR J1740-5340 was identified by D’Amico et al. (2001a) during a systematic search for MSP in GCs carried out with the Parkes radio telescope. The pulsar displays eclipses at a frequency of 1.4 GHz for more than 40% of the 32.5 hr orbital period and exhibits striking irregularities of the radio signal at all orbital phases (D’Amico et al 2001b). This suggests that the MSP is orbiting within a large envelope of matter released from the companion, whose interaction with the pulsar wind could be responsible for the modulated and probably extended X-ray emission detected with CHANDRA (Grindlay et al. 2001, 2002). By using high resolution multiband HST observations and the position of the MSP inferred from radio timing, Ferraro et al (2001b) identified a bright variable star (hereafter COM J1740-5340) as the optical counterpart to the MSP companion, whose optical modulation nicely agrees with the orbital period of the MSP itself. The optical counterpart shows a quite anomalous position in the CMD since it is located at the luminosity of the TO point but it has an anomalous red color (see Figure 20).

As quoted above, in the classical framework of the MSP recycling scenario, the usual companion to a binary MSP should be either a WD or a very light ($0.01 - 0.03 M_{\odot}$), almost exhausted star. None of these scenarios can be applied to COM J1740-5340: it is too luminous to be a WD ($V \sim 16.5$, comparable to the TO stars of NGC6397); moreover its mass ($M \sim 0.2M_{\odot}$), recently constrained by radial velocity observations (see Figure 21), is too high for a very light stellar companion. As a consequence, a wealth of intriguing scenarios have flourished in order to explain the nature of this binary (see Orosz & van Kerkwijk 2003, Grindlay et al. 2002 for a review). In particular, Burderi et al. (2002) suggested that the position of COM J1740-5340 in the CMD (CMD) is consistent with the evolution of an (slightly) evolved Sub Giant Branch (SGB) star orbiting the NS and losing mass. The future evolution of this system will generate a He-WD/MSP pair (see *panel (d)* in Figure 20). COM J1740-5340 could be a star acquired by exchange interaction in the cluster core or alternatively the same star that spun up the MSP and still overflowing its Roche lobe. The latter case suggests the fascinating possibility that PSR J1740-5340 is a new-born MSP, the very first observed just after the end of the recycling process.

This is the first example ever observed of a MSP companion whose light curve is dominated by ellipsoidal variations, suggestive of a tidally distorted star, which almost completely fills (and is still overflowing) its Roche lobe. Thanks to the unusual brightness of the companion ($V \sim 16.5$), this system represents an unique laboratory to study the formation mechanism of binary MSP in GCs, allowing unprecedented detailed spectroscopic observations. In this contest, our group is coordinating a spectro-photometric programme at ESO-Telescopes. In particular a first set of high resolution spectra have been acquired at the *Very Large Telescope* (VLT) with UVES. From these data we obtained a number of interesting results:

- The determination of the radial velocity curve (see Figure 21) allowed an accurate measure of the mass ratio of the system ($M_{PRS}/M_{COM} = 5.83 \pm 0.13$) which suggests a mass of $M_{COM} \sim 0.25M_{\odot}$ by assuming $M_{PRS} \sim 1.4M_{\odot}$. (Ferraro et al 2003b).

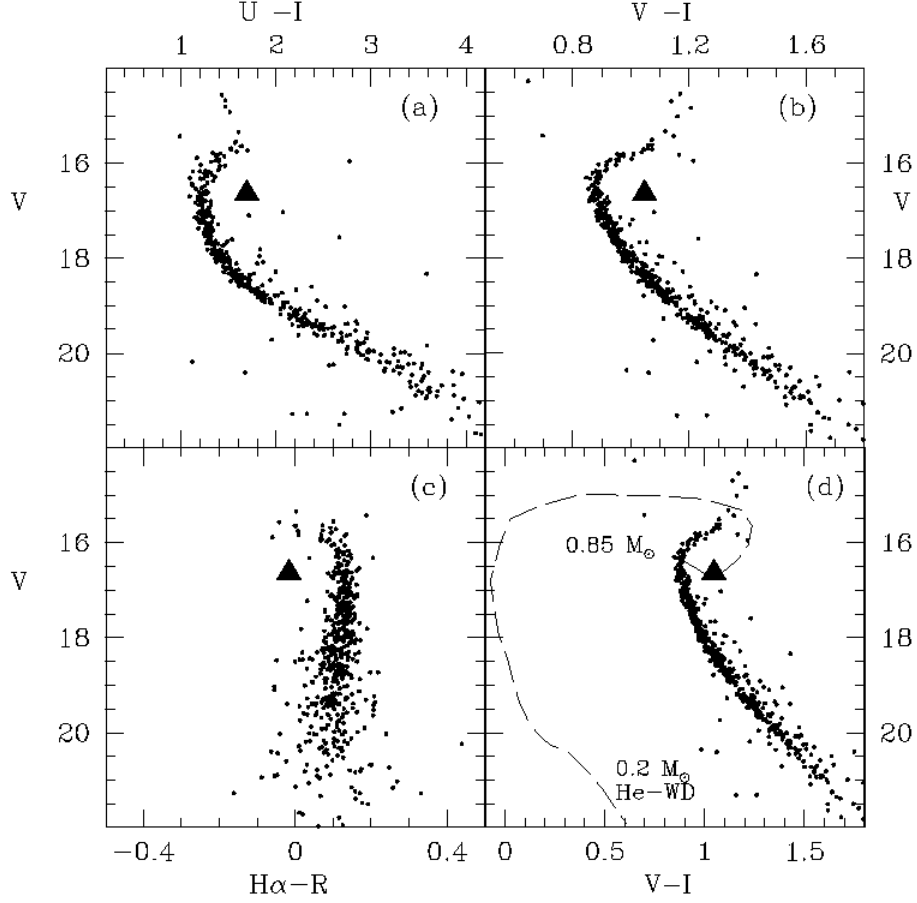


Figure 20. The optical counterpart to the MSP companion in NGC6397. Multiband Color Magnitude Diagram for stars detected in a region around the nominal position of the MSP. The optical counterpart of the MSP companion is marked with a large filled triangle in all panels. In *Panel (d)* the evolution path suggested by Burderi et al. (2002) is shown. (From Ferraro et al (2001b).

- The H_α emission from the system was already noted by Ferraro et al (2001b, see also *Panel (c)* in Figure 20) and fully confirmed by the high-resolution spectra (Sabbi et al 2003a). In particular, the complex structure of the H_α line suggests the presence of a matter stream exaping from the companion towards the NS. Note that because of the radiation flux from the pulsar, the material would never reach the NS surface, creating a cometary-like gaseous tail which feeds the presence of (optically thin) hydrogen gas outside the Roche lobe.
- The unexpected detection of strong He I absorption lines (see Figure 22) implies the existence of a region at $T > 10,000K$, significantly hotter than the rest of the star (Ferraro et al 2003b, Sabbi et al 2003a,b). The intensity of the He I line correlates with the orbital phase, suggesting the presence

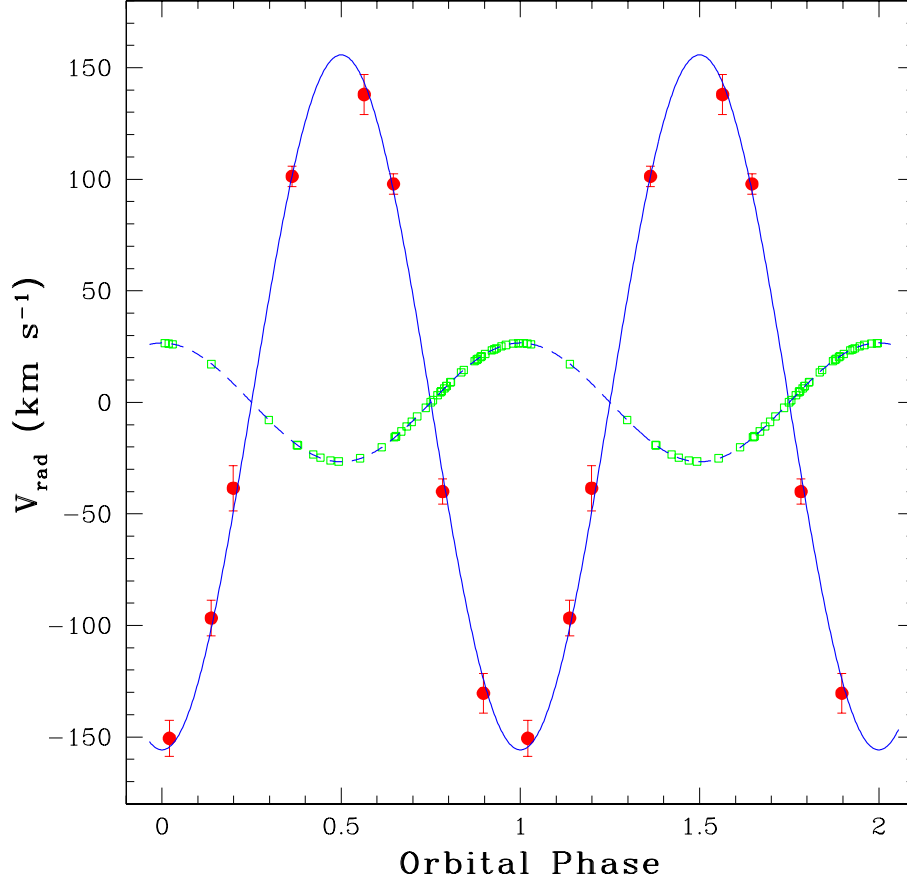


Figure 21. The *large dots* are the radial velocity determinations for COM J1740-5340. The *solid line* represents the best-fit sinusoidal curve. The *small open squares* are the radial velocity determinations for PSR J1740-5340 derived from timing measurements and the radio ephemeris (D’Amico et al. 2001b). The *dotted line* represents the fitted velocity curve of the pulsar. (From Ferraro et al 2003b).

of a region on the companion surface, heated by the millisecond pulsar flux.

- COM J1740-5340 has been found to show a large rotation velocity ($V \sin i = 50 \pm 1 \text{ km s}^{-1}$). The derived abundances are found fully consistent with those of normal unperturbed stars in NGC 6397, with the exception of a few elements (Li, Ca, and C). In particular, the lack of C suggests that the star has been peeled down to regions where incomplete CNO burning occurs (Sabbi et al. 2003b), favoring a scenario where the companion is a SGB star which has lost most of its mass (see also Ergma & Sarna 2003).

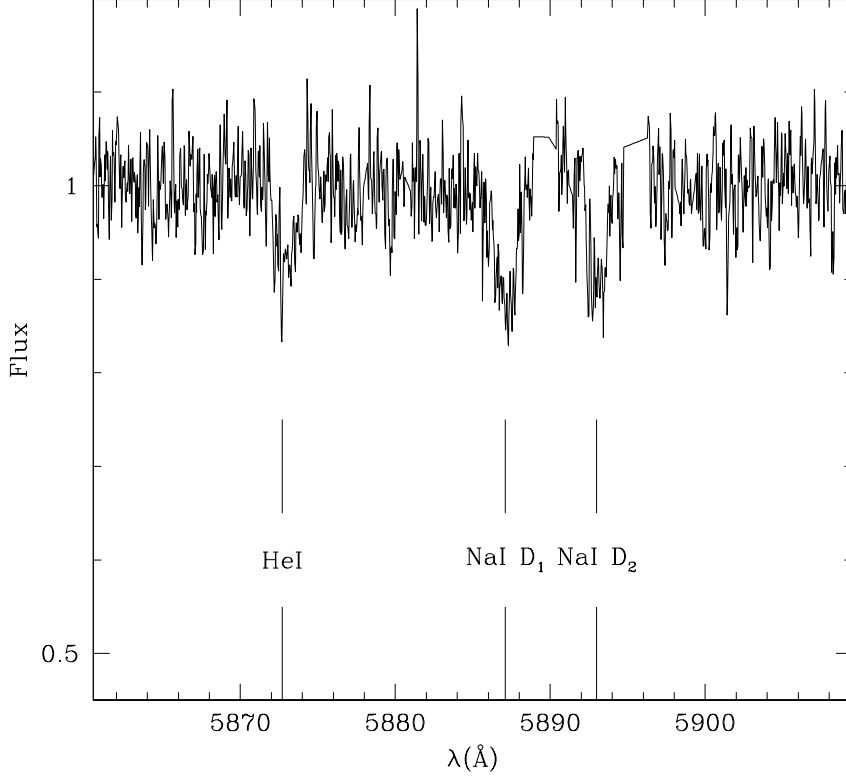


Figure 22. Portion of the normalized spectrum taken at $\phi = 0.02$ in the NaI D lines region (the telluric NaI lines have been removed for clarity). The spectrum has been smoothed with a boxcar of 3 pixels, and not shifted to rest wavelengths; the observed RV is -145.4 km s^{-1} . The HeI absorption line at 5875.6 Å is clearly visible; NaI D lines and the strong He line are also indicated. (From Ferraro et al 2003b).

3.2. The case of NGC6752

Another interesting object has captured our attention: the binary MSP PSR J1911-5958A (hereafter PSR-A), recently discovered in the outskirts of the nearby GC NGC 6752 (D’Amico et al. 2001a). It is located quite far away (at about $6'$) from the cluster optical center. Indeed PSR-A is the more off-centered pulsar among the sample of 41 MSPs with known positions in the parent cluster.

By using deep high-resolution multiband images taken at the ESO VLT we recently identified the optical binary companion to PSR-A (COM-PSR-A, Ferraro et al 2003c). The object turns out to be a blue star whose position in the CMD is consistent with the cooling sequence of a low mass ($M \sim 0.17\text{--}0.20M_{\odot}$), low metallicity Helium WD (He-WD) (see Figure 23, see also Bassa et al 2003).

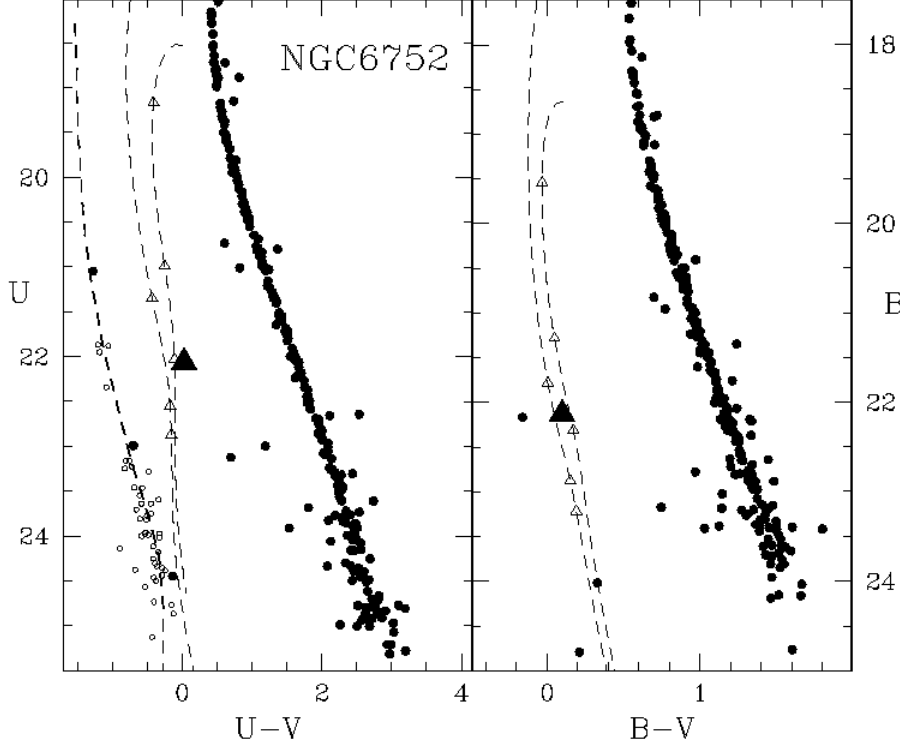


Figure 23. $(U, U - V)$ and $(B, B - V)$ CMDs for the stars identified in a region of $80'' \times 80''$ centered at the nominal position of the PSR J1911-5958A in NGC6752. The optical counterpart to the pulsar companion (COM J1911-5958A) is marked with a *large filled triangles*. The *heavy dashed line* is the CO-WD cooling sequence from Wood (1995); the two *light dashed lines* are the cooling tracks for He WD masses 0.197 and $0.172 M_{\odot}$ (Serenelli et al. 2002). (From Ferraro et al 2003b).

The anomalous position of PSR-A with respect to the GC center suggested that this system has been recently (< 1 Gyr) ejected from the cluster core as the result of a strong dynamical interaction.

3.3. Photometric properties of MSP companion in GCs

The companion to PSR-A is the second He-WD which has been found to orbit a MSP in GCs. Curiously, both objects lie on the same mass He-WD cooling sequence.

Since the first discovery of U_{opt} , in 47 Tuc (Edmonds et al 2001), the zoo of the optical MSP counterparts in GCs is rapidly enlarging. Figure 24 shows a

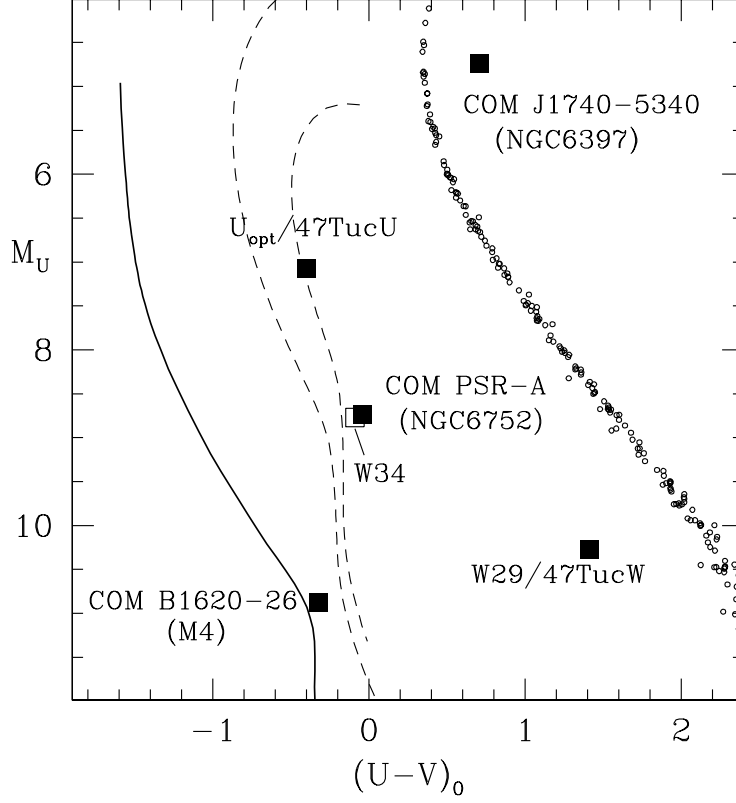


Figure 24. All the optical counterparts to MSP companion detected so far in GCs are plotted (as large filled squares) in the $(M_U, U - V)$ plane. The cooling sequences for He-WD (from Serenelli et al. 2002) and for the CO-WD (from Wood 1995) are also replotted. MS stars of NGC6752 are plotted for reference. (From Ferraro et al 2003b).

comparison of the photometric properties of the available optical identifications of MSP companions hosted in GCs. Note that we also include an additional potential MSP companion (W34 in 47 Tuc) discussed by Edmonds et al. (2003). 2 out of the 5 sources are really peculiar: the bright object in NGC6397 (which is as luminous as the turn off stars and shows quite red colors) and the faint W29 in 47 Tuc, which is also too red to be a He-WD (Edmonds et al 2002). Indeed, U_{opt} and COM-PSR-A lie nearly on the same mass He-WD cooling sequence and W34 in 47 Tuc curiously shares the same photometric properties of COM-PSR-A. Indeed, if confirmed as a MSP companion, W34 would be the third He-WD companion orbiting a MSP in GCs roughly located on the same-mass cooling sequence. If further supported by additional cases, this evidence could confirm

that a low mass $\sim 0.15 - 0.2 M_{\odot}$ He-WD orbiting a MSP is the favored system generated by the recycling process of MSPs in GCs (Rasio et al 2000).

3.4. MSPs as probes of the cluster dynamics

Among the list of the GCs harboring MSP, NGC6752 presents a number of surprising features:

- NGC 6752 hosts 5 known MSP (hereafter PSR A, B, C, D, E, D’Amico et al. 2001; D’Amico et al. 2002).
- As discussed in the previous section, NGC6752 harbors the two most off-centered pulsars (PSR-A and PSR-C) among the sample of MSPs whose position in the corresponding cluster is known.
- In the plane of the sky, the positions of the other 3 known MSPs in the cluster (PSR-B, D, E, all isolated pulsars, see D’Amico et al. 2001a, 2002) are close to the cluster center, as expected from mass segregation in the cluster. D’Amico et al. (2002) found two of them (PSR-B and E) showing large *negative* values of \dot{P} , implying that the pulsars are experiencing an acceleration with a line-of-sight component a_l directed toward the observer and a magnitude significantly larger than the positive component of \dot{P} due to the intrinsic pulsar spin-down.
- By combining HST and wide field observations, Ferraro et al (2003d) constructed the most extended ($0' - 27'$) and complete radial density profile ever obtained for this cluster (see Figure 25). The observed radial density profile shows a significant deviation from a canonical King model in the innermost region, indicating, beyond any doubt, that the cluster core is experiencing the collapse phase. On the basis of this data set Ferraro et al (2003d) also re-determined the center of gravity C_{grav} , which turns out to be $\sim 10''$ S and $\sim 2''$ E of the C_{lum} reported by Djorgovski (1993). Interestingly, the barycenter of the 9 innermost X-ray sources detected by *Chandra* (Pooley et al 2002) is located only $1''.9$ from the new C_{grav} .

On the basis of these new results, Ferraro et al (2003d) suggested two viable explanations of the observed negative \dot{P} : (i) the accelerating effect of the cluster gravitational potential well or (ii) the presence of some close perturber(s) exerting a gravitational pull on the pulsars.

Case (i): Overall effect of the GC potential well The hypothesis that the line-of-sight acceleration of the MSPs with negative \dot{P} is dominated by the cluster gravitational potential has been routinely applied to many globulars. In the case of NGC6752, under the hypothesis that the line-of-sight acceleration of PSR-B and PSR-E are entirely due to the cluster gravitational potential, a $\mathcal{M}/\mathcal{L}_V \sim 6-7$ is inferred (see Figure 26). Collapsed globulars typically show values of $\mathcal{M}/\mathcal{L}_V \sim 2-3.5$ (Pryor & Meylan 1993). Assuming such a value, the expected total mass located within the inner $r_{\perp,B} = 0.08$ pc of NGC 6752 (equivalent to the projected displacement of PSR-B from C_{grav}) would be $\sim 1200-2000 M_{\odot}$. On the other hand, the observed $\mathcal{M}/\mathcal{L}_V \sim 6-7$ implies the existence of an additional $\sim 1500-2000 M_{\odot}$ of low-luminosity matter segregated inside the

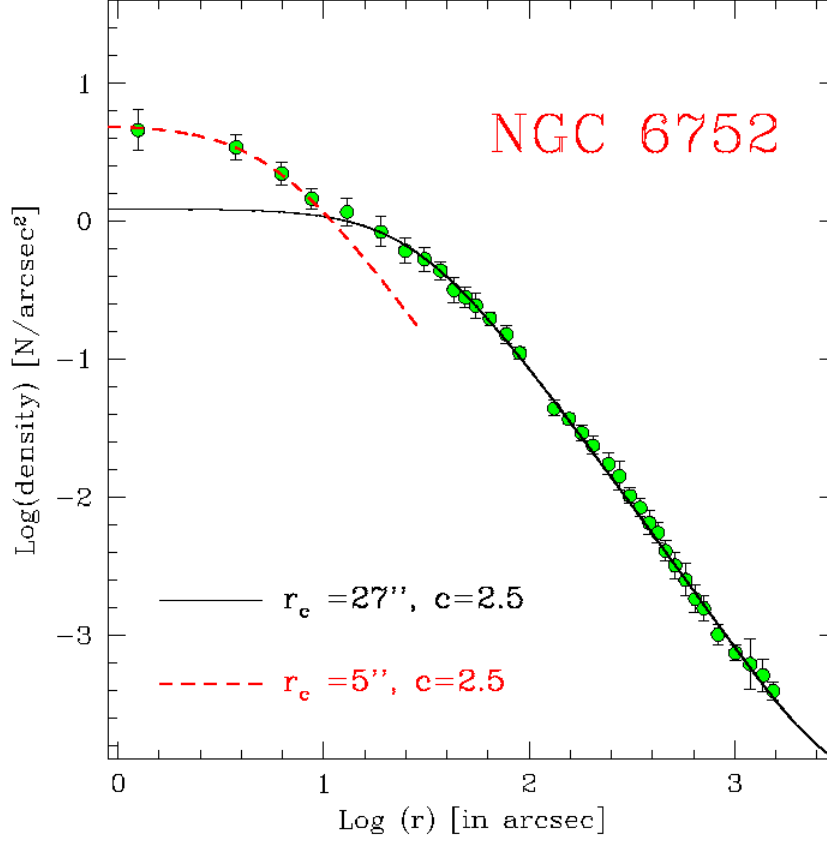


Figure 25. Observed radial density profile with respect to the adopted C_{grav} . The solid line is the best fit King model ($r_c = 28''$ and $c = 1.9$) to the outer points (that is, for distance larger than $10''$ from the cluster center). The King model has been combined with a constant star density of $0.25 \text{ stars arcmin}^{-2}$ in order to account for the flattening of the density profile in the extreme outer region ($r > 16.5$) of the cluster. The dashed line is the best fit King model to the 4 innermost points. (From Ferraro et al 2003d).

projected radius $r_{\perp,B}$. This extra amount of mass cannot be a relatively massive ($> 10^3 M_{\odot}$) black hole (BH), since it would produce a central power-law cusp in the radial density profile, which is not observed (see Figure 25). The high $\mathcal{M}/\mathcal{L}_V$ ratio could be more likely due to a very high central concentration of dark remnants of stellar evolution, like NS and heavy ($\sim 1.0 M_{\odot}$) WD, which sank into the NGC 6752 core during the cluster dynamical evolution (as also proposed for M15 by Gerssen et al. 2003 and Baumgardt et al. 2003).

Case (ii): Local perturbator(s) One can imagine as an alternative possibility that the acceleration imparted to PSR-B and PSR-E is due to some local perturbators. Could a *single* object, significantly more massive than a typical

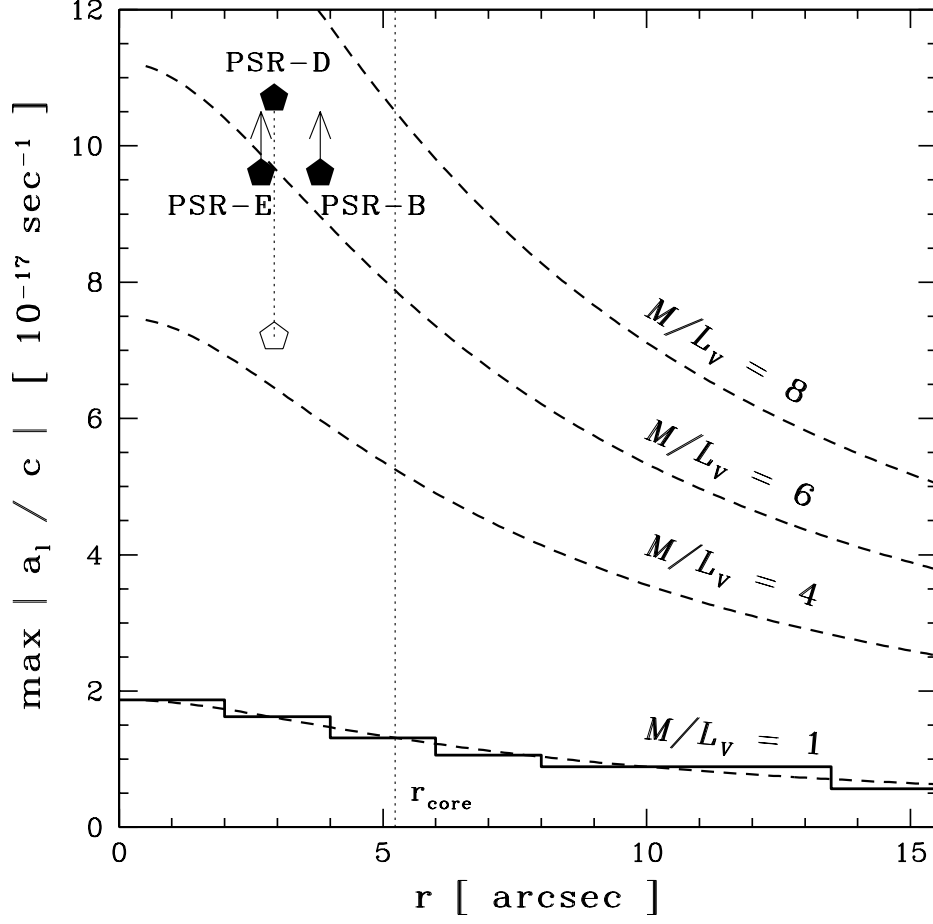


Figure 26. Maximum line-of-sight acceleration $|a_{l_{max}}/c| = |\dot{P}/P|$ versus radial offset with respect to the center of NGC 6752. The histogram represents the prediction based on the star density profile (normalized to the central surface brightness) assuming a unity mass-to-light ratio. The dashed lines are analytical fits to the optical observations, labeled according to the adopted mass-to-light ratio. The measured values of \dot{P}/P (filled pentagons, D’Amico et al. 2002) in the two MSPs with negative \dot{P} (PSR-B and E) can be reproduced only for $\mathcal{M}/\mathcal{L}_V > 6 - 7$. The open pentagons show our best guessed range of maximum $|a_l/c|$ for PSR-D: the upper value is calculated assuming a negligible intrinsic positive \dot{P}_{sd} ; the lower value is estimated taking into account intrinsic \dot{P}_{sd} from the observed scalings between X-ray luminosity and spin-down power for MSPs (see D’Amico et al. 2002 and reference therein). (from Ferraro et al 2003d).

star in the cluster simultaneously produce the accelerations detected both in PSR-B and PSR-E? Recently, Colpi, Possenti & Gualandris (2002) suggested the presence of a binary BH of moderate mass ($M_{bh+bh} \sim 100\text{--}200 M_\odot$) in the center of NGC 6752, in order to explain the unexpected position of PSR-A in the outskirts of the cluster. The projected separation of PSR-B and PSR-E is

only $d_{\perp} = 0.03$ pc. A binary BH of total mass $M_{\text{bh+bh}}$, approximately located in front of them within a distance of the same order of d_{\perp} , could accelerate both pulsars without leaving any observable signature on the cluster density profile. As the BH binarity ensures a large cross section to interaction with other stars, the recoil velocity v_{rec} due to a recent dynamical encounter could explain the offset position (with respect to C_{grav}) of the BH. However this scenario has low probability to occur: indeed, placing the BH at random within the core gives roughly a 1% chance that it would land in the right location to produce the observed pulsar accelerations.

Acknowledgments. It is a pleasure to thank Bob Rood, Alison Sills, Michela Mapelli, Monica Colpi, Giacomo Beccari, Elena Sabbi, Andrea Possenti, Nichi D’Amico and the many other friends who are collaborating to this project. This research was supported by the *Ministero della Istruzione dell’Università e della Ricerca* (MIUR). A special thanks to Livia for her lovely support.

References

- Auriere, M. & Ortolani, S. 1989, A&A, 221, 20 (AO89)
- Bailyn, C. D., 1995, ARA&A, 33, 133
- Bassa, C. G., Verbunt, F., van Kerkwijk, M. H., & Homer, L. 2003, A&A, 409, L31
- Baumgardt, H., Hut, P., Makino, J., McMillen, S., & Portegies Zwart S. 2003, ApJ, 582, L21
- Bellazzini, M., Fusi Pecci, F., Messineo, M., Monaco, L., & Rood, R. T. 2002, AJ, 123, 1509
- Bolte, M., Hesser, J.E., Stetson, P.B. 1993, ApJ, 408, L89
- Buonanno, R., Corsi, C.E., Buzzoni, A., Cacciari, C., Ferraro, F.R., Fusi Pecci, F. 1994, A&A, 290, 69
- Burderi, L., D’Antona, F., Burgay, M., 2002, ApJ, 574, 325
- Colpi, M., Possenti, A., & Gualandris, A. 2002, ApJ, 570, L85
- Colpi, M., Mapelli, M., & Possenti, A. 2003, ApJ, 599, 1260
- D’Amico, N., Lyne, A. G., Manchester, R. N., Possenti, A. & Camilo, F. 2001a, ApJ, 548, L171
- D’Amico, N., Possenti, A., Manchester, R. N., Sarkissian, J., Lyne, A. G. & Camilo, F. 2001b, ApJ, 561, L89
- D’Amico, N., Possenti, A., Fici, L., Manchester, R. N., Lyne, A. G., Camilo, F., & Sarkissian, J. 2002, ApJ, 570, L89
- Davies, M. B., Piotto, G. & De Angeli, F., 2004, MNRAS, 349, 129
- Djorgovski, S., & King, I. R. 1986, ApJ, 305, L71
- Djorgovski, S. 1993, in ASP Conf. Ser. 50, Structure and Dynamics of Globular Clusters, ed. S. G. Djorgovski & G. Meylan (San Francisco: ASP), 373 (D93)
- Djorgovski, S., & Meylan, G. 1993, in ASP Conf. Ser. 50, Structure and Dynamics of Globular Clusters, ed. S. G. Djorgovski & G. Meylan (San Francisco: ASP), 325 (DM93)
- Edmonds, P. D., Gilliland, R. L., Heinke, C. O., Grindlay, J. E., & Camilo, F. 2001
- Edmonds, P. D., Gilliland, R. L., Camilo, F., Heinke, C. O., & Grindlay, J. E. 2002a, ApJ, 579, 741
- Edmonds, P. D., Gilliland, R. L., Heinke, C. O., & Grindlay, J. E. 2003, ApJ, 596, 1177
- Ergma, E., Sarna, M.J., 2003, A&A, 399, 237
- Ferraro F. R., & Paresce, F., 1993, AJ, 106, 154
- Ferraro F. R., Pecci F. F., Cacciari C., Corsi C., Buonanno R., Fahlman G. G., Richer H. B., 1993, AJ, 106, 2324 (F93)
- Ferraro, F. R., Fusi Pecci, F., & Bellazzini, M. 1995, A&A, 294, 80 (FFB95)
- Ferraro, F. R., et al. 1997a, A&A, 324, 915 (F97)

- Ferraro, F. R., paltrinieri, B., Fusi Pecci, F., Cacciari, C., Dorman, B., Rood, R.T., 1997, *ApJ*, 484, L145
- Ferraro, F. R., Paltrinieri, B., Fusi Pecci, F., Rood, R. T., & Dorman, B. 1998, *ApJ*, 500, 311
- Ferraro, F. R., Paltrinieri, B., Rood, R. T., & Dorman, B. 1999, *ApJ*, 522, 983 (F99)
- Ferraro, F. R., Paltrinieri, B., Paresce, F., and De Marchi, G., 2000, *ApJ*, 542, L29
- Ferraro, F.R., D'Amico, N., Possenti, A., Mignani, R.P., Paltrinieri, B. 2001a, *ApJ*, 561, 337
- Ferraro, F. R., Possenti, A., D'Amico, N., & Sabbi, E. 2001b, *ApJ*, 561, L93
- Ferraro, F. R., Bellazzini, M., Pancino, E. 2002, *ApJ*, 573, L95
- Ferraro F. R., Sills A., Rood R. T., Paltrinieri B., Buonanno R., 2003a, *ApJ*, 588, 464 (F03)
- Ferraro, F. R., Sabbi, E., Gratton, R., Possenti, A., D'Amico, N., Bragaglia, & A., Camilo, F. 2003b, *ApJ*, 584, L13
- Ferraro, F. R., Possenti, A., Sabbi, E., D'Amico, N., 2003c, *ApJ*, 596, L211
- Ferraro, F. R., Possenti, A., Sabbi, E., Lagani, P., Rood, R. T., D'Amico, N., & Origlia, L. 2003d, *ApJ*, 595, 179
- Ferraro F. R., Beccari G., Rood R. T., Bellazzini M., Sills A., Sabbi E., 2004a, *ApJ*, 603, 127
- Ferraro, F. R., Sollima, A., Pancino, E., Bellazzini, M., Origlia, L., Straniero, O., Cool, A., 2004b, *ApJ*, 603, L81
- Ferraro, F. R., Rood, Sollima, A., Rood, R.T., Origlia, L., Pancino, E., Bellazzini, M., 2005, *ApJ*, in press
- Fusi Pecci, F., Ferraro, F.R., Corsi, C.E., Cacciari, C., & Buonanno, R. 1992, *AJ*, 104, 1831
- Gerssen, J., van der Marel, R. P., Gebhardt, K., Guhathakurta, P., Peterson, R. C., & Pryor, C. 2003, *AJ*, 125, 376
- Grindlay, J. E., Heinke, C. O., Edmonds, P. D., Murray, S. S. & Cool, A. 2001, *ApJ*, 563, L53
- Grindlay, J. E., Camilo, F., Heinke, C. O., Edmonds, P. D., Cohn, H., Lugger, P., 2002, *ApJ*, 581, 470
- Guhathakurta, P., Yanny, B., Bahcall, J.N., Schneider, D.P. 1994, *AJ*, 108, 1786
- Guhathakurta, P., Yanny, B., Schneider, D. P., & Bahcall, J. N. 1996, *AJ*, 111, 267
- Lee, Y. W., Joo, J. M., Sohn, Y. J., Rey, S. C., Lee, H. C. & Walker, A. R., 1999, *Nature*, 402, 55
- Mapelli, M., Sigurdsson, S., Colpi, M., Ferraro, F. R., Possenti, A., Rood, R. T., Sills, A., Beccari, G., 2004, *ApJ*, 605, L29
- Meylan, G., & Heggie, D. C. 1997, *A&A Rev.*, 8, 1
- Orosz, J.A., van Kerkwijk, M. H., 2003, *A&A*, 397, 237
- Pancino, E., Ferraro, F. R., Bellazzini, M., Piotto, G. & Zoccali, M., 2000, *ApJ*, 534, L83
- Piotto, G., et al. 2004, *ApJ*, 604, L109
- Rasio, F.A., Pfahl, E.D., Rappaport, S., 2000, *ApJ*, 532, L47
- Renzini, A., Fusi Pecci, F. 1988, *ARA&A*, 26, 199
- Sabbi, E., Gratton, R., Ferraro, F. R., Bragaglia, A., Possenti, A., D'Amico, N., Camilo, F., 2003a, *ApJ*, 589, L41
- Sabbi, E., Gratton, R., Bragaglia, A., Ferraro, F. R., Possenti, A., Camilo, F., D'Amico, N., 2003b, *A&A*, 412, 829
- Sabbi, E., Ferraro, F. R., Sills, A., Rood, R.T., 2004, *ApJ*, 617, 1296
- Shara, M. M., Saffer, R. A., & Livio, M. 1997, *ApJ*, 489, L59
- Serenelli, A. M., Althaus, L. G., Rohrmann, R. D., & Benvenuto, O. G. 2002, *MNRAS*, 337, 1091
- Sigurdsson, S., & Phinney, S. 1993, *ApJ*, 415, 631
- Sigurdsson, S., Davies, M.B., Bolte, M., 1994, *ApJ*, 431, L115
- Sigurdsson, S., & Phinney, E. S. 1995, *ApJS*, 99, 609

- Sigurdsson, S., Richer, H. B., Hansen, B. M., Stairs, I. H., & Thorsett, S. E. 2003, *Science*, 301, 193
- Sollima, A., Ferraro, F. R., Pancino & E., Bellazzini, M., 2005, *MNRAS*, 357, 265
- Trager, S. C., King, I. R., & Djorgovski, S. 1995, *AJ*, 109, 1912
- Verbunt, F., 2003 “New Horizons in Globular Cluster Astronomy”, *ASP Conference Proceedings*, 296, 245
- Zaggia, S. R., Piotto, G. & Capaccioli M., 1997, *A&A*, 327, 1004